Asian Journal of Pharmaceutical Sciences 15 (2020) 617–636

Available online at www.sciencedirect.com

ScienceDirect

journal homepage: www.elsevier.com/locate/AJPS

Original Research Paper

A stepwise optimization strategy to formulate *in situ* gelling formulations comprising fluconazole-hydroxypropyl-beta-cyclodextrin complex loaded niosomal vesicles and Eudragit nanoparticles for enhanced antifungal activity and prolonged ocular delivery

Heba Elmotasem[a,*], *Ghada E.A. Awad*[b]

[a] *Pharmaceutical Technology Department, National Research Centre, Cairo 12622, Egypt*
[b] *Chemistry of Natural and Microbial Product Department, National Research Centre, Cairo 12622, Egypt*

ARTICLE INFO

Article history:
Received 14 June 2019
Revised 22 August 2019
Accepted 30 September 2019
Available online 24 December 2019

Key words:
Fluconazole
Ocular
Eudragit nanoparticles
Cyclodextrin
Niosomes
In situ gel

ABSTRACT

Fungal keratitis and endopthalmitis are serious eye diseases. Fluconazole (FL) is indicated for their treatment, but suffers from poor topical ocular availability. This study was intended to improve and prolong its ocular availability. FL niosomal vesicles were prepared using span 60. Also, polymeric nanoparticles were prepared using cationic Eudragit RS100 and Eudragit RL100. The investigated particles had adequate entrapment efficiency (EE%), nanoscale particle size and high zeta potential. Subsequently, formulations were optimized using full factorial design. FL-HP-β-CD complex was encapsulated in selected Eudragit nanoprticles (FL-CD-ERS1) and niosmal vesicles. The niosomes were further coated with cationic and bioadhesive chitosan (FL-CD-Nios-ch). EE% for FL-CD-ERS1 and FL-CD-Nios-ch formulations were 76.4% and 61.7%; particle sizes were 151.1 and 392 nm; also, they exhibited satisfactory zeta potential +40.1 and +28.5 mV. *In situ* gels were prepared by poloxamer P407, HPMC and chitosan and evaluated for gelling capacity, rheological behavior and gelling temperature. To increase the precorneal residence time, free drug and selected nano-formulations were incorporated in the selected *in situ* gel. Release study revealed sustained release within 24 h. Permeation through excised rabbits corneas demonstrated enhanced drug flux and large $AUC_{0\text{-}6h}$ in comparison to plain drug. Corneal permeation of selected formulations labeled with Rhodamine B was visualized by Confocal laser microscopy. Histopathological study and *in vivo* tolerance test evidenced safety. *In vivo* susceptibility test using *Candida albicans* depicted enhanced growth inhibition and sustained effect. In this study the adopted stepwise optimization strategy combined cylodextrin complexation, drug nano-encapsulation and loading within thermosenstive *in situ* gel. Finally, the developed innovated formulations displayed boosted corneal permeation, enhanced antifungal activity and prolonged action.

* Correponding author. Pharmaceutical Technology Department, National Research Centre, El-Buhouth Street, Dokki, Cairo 12622, Egypt. Tel.: +20 2 33335456.
E-mail address: almotasem85@hotmail.com (H. Elmotasem).
Peer review under responsibility of Shenyang Pharmaceutical University.

https://doi.org/10.1016/j.ajps.2019.09.003

1. Introduction

Infections by different fungal species is one of the most serious and challenging problems affecting the eye. The incidence of fungal infections increases in immune-compromised patients after organ transplantation, patients who receive chemotherapy and in intensive care units. Ocular fungal infections can be a result of eye traumas or surgeries complications. Additionally, the increasing number of people who wear contact lenses, either for medical or cosmetic reasons, without proper hygiene lead to escalation of this problem. In developing countries and hot climates ocular fungal infections account for nearly 50% of microbial keratitis [1]. Fungal infections can affect both anterior and posterior eye chambers in the case of endopthalmitis. The most common sites for fungal infections of eyes are cornea, retina and vitreous. Also, they can involve other periocular tissues including lacrimal apparatus, conjunctiva, sclera, eyelids and bony orbit [2]. If the infection was inadequately treated, corneal transplantation or vitrectomy might be required. Fungal infections can lead to irreversible sight damage or even blindness within days of the disease onset.

Efficient medical treatment of ophthalmic mycotic infections relies on the drug antifungal spectrum, contact duration with the affected tissue and achieved concentration in the targeted sites [3]. The physicochemical and pharmacokinetic properties of the drug are the major determinants in this aspect [4]. Fluconazole (FL), a synthetic fluorinated bis-triazole derivative, is one of the most important antimycotic agents with a broad spectrum and advantageous physicochemical properties. It is widely used for prophylaxis and treatment purposes for several *candidal* infections. It has intermediate molecular weight and short $T_{1/2}$ in eyes [5]. It has better aqueous solubility in comparison to other azole derivatives. Also, it has better safety profile compared to other antifungal analogues. These characteristics encourage ophthalmologists to prescribe it as a first line in *Candidal infections* treatment. But still it is a slightly soluble drug which is confronted with the problems of low bioavailability as the ophthalmic aqueous eye drops. The constraining barrier mechanisms of different eye layers, blinking, dynamic rapid tear turnover rate and the nasolarcrimal drainage into systemic circulation permit less than 5% of an applied topical drug dose of conventional aqueous eye drops to get access to intraocular tissues [6]. It was found that following local application of FL eye drops, the aqueous humor concentration was below the minimal inhibitory concentration of FL for most eumycetes [7]. This dictates the use of oral systemic therapy or invasive routes like subconjunctival injections and intraocular injections. Also, this mandates adopting more conservative therapeutic interventions like using combinations of two or more antimycotic drugs concurrently. These interventions increase the liability to several side effects and different drug interactions. Therefore, it is crucial to increase the bioavailability of FL eye drops for effective control of mycotic keratitis and endophthalmitis infections.

Several approaches have been carried out aiming to enhance the ocular availability of FL like entrapping in liposomes [8,9], and using lyophilized liposomes after reconstitution for increasing the physical stability of the drug [10]. Also, combined permeation enhancers like menthol and borneol were used for augmenting the drug topical ocular permeation [11]. Spanlastics, that contained spans as edge activators, were studied [12]. Also, microemulsions use was investigated [13]. Furthermore, different studies were conducted for increasing FL ocular residence time and enhancing its bioavailability. These studies included formulating poloxomer/chitosan *in situ* gel [14] and other thermo-responsive *in situ* gel formulations [15], pH-triggered nano-emulsified *in situ* gel [16] and chitin nanogels [17]. Implants containing FL-beta-cyclodextrin complex and *in situ* gel comprising FL cyclodextrin complexes were studied [18]. Also, niosomes integrated *in situ* gel was investigated [19]. The entrapment within Eudragit RS and RL nanoparticles (NPs) was attempted [20]. Also, nanosized hyalugel integrated liposomes and gel in core carbosomes were prepared and evaluated for enhancing and prolonging the drug effect [21,22]. The results of aforementioned studies were promising.

However, due to the dramatic increase in the fungal resistance to drugs and the epidemiologic increase in the invasive fungal infections, there is a vital increasing need for exploiting new delivery systems that can increase the drug ocular availability and avoid the mechanisms of fungal resistance [23]. Fungal resistance is a consequence of the long term use of the antifungal drug for prophylaxis purposes or inadequate treatment caused by either low drug concentration or early discontinuation of medication due patient incompliance. Resistance can also occur as a result of drug efflux mechanisms or the impermeability of cell membrane for drug molecules, enzymatic inactivation and degradation of the drug outside fungal cell [24]. This can lead to therapeutic failure which dictates more aggressive long term treatment. Thus, it mandates exploiting new effective alternative drug delivery systems [25].

Future trends in treating ocular diseases affecting anterior or posterior eye segments will be more focused on the use of noninvasive delivery routes and colloidal carriers that are based on FDA approved excipients that can deliver adequate therapeutic drug concentration to both the anterior and posterior eye segments [26,27]. Cyclodextrins are widely used additives in ophthalmic formulations. They were used to increase aqueous solubility, stability, bioavailability, and decrease drug irritation of ophthalmic drugs [26,27]. They have been broadly investigated as an inimitable pharmaceutical excipient for the last few decades and is still being explored for new applications [28–33]. Recently, combining cyclodextrin complexes within different nanocarriers has got extensive consideration in several studies and has revealed potentiality as an enabling tool in drug delivery systems [34–38].

The aim of the present work is to develop a safe ophthalmic delivery system for the antimycotic drug FL with enhanced ocular permeation and increased retention time. This can be achieved by formulating bioadhesive FL nanosized systems to be loaded within thermosenstive *in situ* gels. A stepwise optimization of FL loaded niosomal vesicles and Eudragit RS and RL NPs was done. The impact of incorporating the drug in the form of hydroxypropyl-beta-cyclodextrin (HP-β-CD) complex in the selected optimized nano-formulations

was exploited. Innovating delivery systems, combining nanovesicles and cyclodextins as drug carriers can enable effective therapy and minimize side effects. Finally, these formulations were blended in thermosensitive *in situ* gelling formulation. These formulations can be administered accurately in a liquid form and transferred into gel on contacting the eye surface. Thus, they increase contact time between the eye surface and enhance drug permeation into the eye compartments, decrease its nasolacrimal drainage and unwanted systemic absorption. Finally, these formulations can improve patient compliance by decreasing dosing frequency and lead to better control of the disease.

2. Materials and methods

2.1. Materials

FL was kindly provided by Sedico pharmaceutical corporation (Egypt). Eudragit RS100 and Eudragit RL100 were obtained from Evonik, Rohm GmbH Pharma Polymers (Germany). Span 60, cholesterol, HP-β-CD, hydroxypropyl methyl cellulose (HPMC, 86 kDa), Kolliphor P407 (Poloxamer 407) and Rhodamine B (Rh B) were obtained from Sigma-Aldrich Co., (USA). Chitosan powder with a 85% degree of deacetylation and molecular weight of 6×10^5 Da was purchased from Alfa Aesar Co., (USA). Polyvinyl alcohol (PVA) with 1700–1800° of polymerization was obtained from Loba, Chemie, Pvt. Ltd. (Mumbai, India). Dichloromethane, methanol and acetone were purchased from Fisher Scientific (UK). Glacial acetic acid was obtained from El Nasr Pharmaceutical Chemicals Co., (Egypt). All other chemical reagents used in this study were of analytical grade.

2.2. Preparation of FL loaded niosomes

FL loaded niosomes were prepared by thin film hydration method [39]. Briefly, 100 mg mixture of Span 60 and cholesterol at a molar ratio 2:1 along with 25 mg of FL were dissolved in an organic solvent mixture comprising 10 ml dichloromethane and 5 ml methanol in a 100 ml rotary evaporator flask. The resultant solution was evaporated under reduced pressure at 60 ± 2 °C, to form a thin film on the flask wall using the rotary evaporator (Heidolph, Germany). The thin film was hydrated with 10 ml phosphate buffer (pH 7.4) at 60 ± 2 °C and rotation (150 rpm) for 30 min followed by sonication for 5 min. The resultant dispersion was left overnight in the refrigerator for vesicle maturation before separation.

2.3. Preparation of FL loaded eudragit NPs

FL loaded Eudragit NPs were prepared using nanoprecipitation technique which is also known as the solvent displacement method [40]. Drug and polymer were co-dissolved by sonication, in a mixture of organic solvents which comprises acetone and methanol at 1:1 ratio. This organic phase was slowly injected into the aqueous phase under magnetic stirring at 1500 rpm. The aqueous phase contains 0.75% polyvinyl alcohol (PVA) as a stabilizer. A fixed ratio (1:3) was used for organic phase (solvent) to aqueous phase (non solvent). Spontaneous formation of NPs was detected. The clear aqueous solution turned to bluish white opalescent dispersion. Stirring was continued for 6 h to evaporate the organic solvent. Finally, to insure complete elimination of any residual organic solvents, the dispersion was evaporated under reduced pressure at 60 ± 2 °C by the rotary evaporator (Heidolph, Germany). Then the resultant dispersion was adjusted to volume and sonicated for 5 min.

2.4. Determination of FL entrapment efficiency

The drug loaded niosomes or NPs were separated from the un-entrapped drug by cooling centrifugation 9000 rpm at 4 °C for 1 h using cooling centrifuge (Hanil Co., Union 32R, Korea). The drug loaded NPs were collected then re-suspended in phosphate buffer saline pH 7.4. NPs were separated again by centrifugation as mentioned above for further 30 min. This washing procedure was repeated twice. All the resulting supernatants were collected and assayed for the free un-entrapped drug spectrophotometrically at 261 nm. The drug encapsulation efficiency (EE%) was calculated according to this equation:

$$EE\% = (\text{Total drug amount} - \text{Free drug amount}) / (\text{Total drug amount}) \times 100.$$

2.5. Determination of vesicles size, poly dispersity index and zeta potential

Size and poly dispersity index (PDI) of the prepared niosomal vesicles and Eudragit NPs were determined using dynamic light scattering by ZETA Sizer (Malvern Instruments, Ltd Nano Series ZS90, UK). HE-NE laser beam at 632 nm wavelength was employed at 25 °C and an angle equals 90°. The investigated preparations were diluted using double distilled water at a ratio of 1:20 (v/v). PDI was used to measure the size distribution uniformity. The measurements were done in triplicates from independent samples. Zeta potential of the investigated niosomes and Eudragit NPs was determined using ZETA Sizer (Malvern Instruments, Ltd Nano Series ZS90, UK). It measures the potential range −120 to +120 V. The samples were diluted using double distilled water at a ratio of 1:20 (v/v). Measurements were carried in triplicates.

2.6. Optimization of FL loaded Eudragit NPs

FL loaded Eudragit NPs were optimized using a $2^1 \times 3^1$ full factorial experimental design for elucidating the impact of different formulation variables. This was conducted using Design-Expert® 7 software (Stat-Ease,Inc., Minneapolis, USA). Independent variables were the type of Eudragit polymer (X1,A) and the amount of used polymer (X2,B) (Table 1). Particle size (Y1), zeta potential (Y2) and EE% (Y3) were selected as dependent variables. Table 2 shows the composition of prepared formulations. The level of significance of the investigated factors and their interaction on the dependent responses were estimated using ANOVA test.

Table 1 – The Independent variables and observed responses employed in the full factorial design of the fluconazole loaded Eudragit RS100 and Eudragit RL100 nanoparticles. Data represented as mean ± SD ($n = 3$).

Formulation code		Polymer type	Amount (mg)	Drug/polymer ratio	Particle size (nm)	PDI	Zeta potential (mV)	EE%
Eudragit NPs	FLERS1	RS100	100	1:4	107.6 ± 12	0.27	42.6 ± 2	75.3 ± 4
	FLERS2		200	1:8	170.0 ± 10	0.39	44.3 ± 6	75.0 ± 8
	FLERS3		300	1:12	187.4 ± 14	0.41	37.6 ± 5	77.1 ± 10
	FLERL1	RL100	100	1:4	176.6 ± 21	0.43	42.7 ± 3	68.6 ± 7
	FLERL2		200	1: 8	182.4 ± 19	0.55	44.2 ± 7	70.2 ± 11
	FLERL3		300	1:12	234.3 ± 16	0.49	40.6 ± 5	69.3 ± 16
FLNios		–	–	–	209.0 ± 35	0.71	−36.0 ± 4	67.4 ± 9

Table 2 – Full factorial $2^1 \times 3^1$ design employed for optimizing fluconazole loaded Eudragit RS100 and Eudragit RL100 nanoparticles.

	Level		
	Low −1	Medium 0	High +1
X1(A) type of Eudragit	Eudragit RS		Eudragit RL
X2 (B) amount (mg)	100	200	300
Dug to polymer ratio	(1:4)	(1:8)	(1:12)
Response dependent variable		Constrains	
Y1 particle size		Minimize	
Y2 zeta potential		Maximize	
Y3 entrapment efficiency		Maximize	

2.7. *Preparation of FL-HP-β-CD inclusion complex*

FL-HP-β-CD inclusion complex was prepared by kneading method at a drug: cyclodextrin molar stochiometric ratio 1:1 [41]. The mixture was kneaded thoroughly with a minimum amount of water to obtain a paste. Then the mixture was dried under vacuum at room temperature in presence of phosphorus pentoxide as a drying agent [42,43].

2.8. *Preparation of Eudragit NPs and niosomal vesicles incorporating FL in the form of FL-HP-β-CD complex*

The same techniques were used as adopted in Sections 2.2 and 2.3, except for that the equivalent amount of FL was incorporated in the form of drug-cyclodextrin complex.

2.9. *Coating of the optimized niosomal vesicles*

The separated niosomal vesicles were suspended in 0.2% chitosan solution and stirred for 1 h. The coated niosomes were separated by centrifugation. [44].

2.10. *Characterization of selected prepared niosomal and Eudragit NPs*

2.10.1. *Estimation of the particle size, zeta potential and EE%*

The particle size, zeta potential and EE% were estimated for the prepared NPs comprising FL-HP-β-CD complex using the same techniques as adopted in Sections 2.5 and 2.6.

2.10.2. *Transmission electron microscopy study and scanning electron microscopy*

The morphologic examination of selected formulations was performed by transmission electron microscopy (TEM, JEOL Co., JEM-2100, Japan). The samples were diluted at a ratio 1:20 using bi-distilled water. A drop from each of the investigated samples was put on carbon coated copper grid and stained with 2% phosphotungestic acid and left to dry before investigation. The selected investigated samples were lyophilized, then the surface characteristics of the prepared NPs were examined using FEI Quanta FEG 250 scanning electron microscope (SEM). Gold sputtering was done using sputter coater Edwards S150.

2.10.3. *Fourier transform infrared spectroscopy (FTIR) and X-ray diffractometry*

The IR spectra were determined for plain FL, HP-β-CD, FL-HP-β-CD complex, the prepared niosomes and Eudragit NPs JASCO, FT/IR 460 plus. X-ray diffraction patterns were investigated for the selected formulations using (Brukur D8 Advance, Germany). Target = CuKα with secondary monochrometer. It was operated 45 KV and 40 MA.

2.11. *Preparation of thermosenstive in situ gel*

In situ gel formulations were prepared using Poloxamer 407 by adopting the cold method. The weighed amount of polymer was slowly added to bi-distilled cold water under continuous stirring and left overnight in the refrigerator at nearly 4 °C for complete swelling. Regarding the formulations containing chitosan or chitosan/HPMC blend, the chitosan powder was firstly dissolved in 0.5% (w/v) acetic acid solution using a magnetic stirrer at room temperature. Also, the required amount of HPMC was dissolved by continuous stirring at room temperature then allowed to cool in the refrigerator at 4 °C before adding Poloxamer. Afterwards, the required amount of Poloxamer 407 powder was added to the cooled aqueous solutions of chitosan or chitosan/HPMC blend and stored overnight in the refrigerator at 4 °C for complete swelling.

2.12. Evaluation of the in situ gel

To simulate *in vivo* phase change process, the *in situ* gel formulations were evaluated after dilution with simulated tear fluid (STF) in a ratio of 50:7. STF contained 0.200 g sodium bicarbonate, 0.670 g sodium chloride, 0.008 g calcium chloride di-hydrate and purified water up to 100 g.

2.12.1. Measurement of sol–gel phase transition temperature

Tube inversion method was used to determine the sol–gel phase transition temperature [45]. Briefly, a capped test tube containing about 2 ml of *in situ* gel formula, was kept refrigerated at 4 °C. Then, it was transferred to a water bath and the temperature was raised up to 37 °C. The formula was observed for gelling by inverting the test tube at periodic intervals. The gelling temperature was noted when there was no flow or change in the meniscus occurred when the test tube was inverted through 90°.

2.12.2. Gelling capacity determination

The gelling capacity of the investigated formulations was assessed by visually examining a drop of the formulation when inserted to a vial containing 2 ml simulated tear fluid kept at 35 °C. The gelling capacity was determined by assessing the time taken for gel formation and the time taken for its dissolution [46]. The evaluation is graded as follows: no gelling: −; gel formation after few minutes and remains for short time: +; gel formation immediately and dissolved after few hours: ++; gel formation immediately and dissolves after extended period of hours: +++.

2.12.3. Rheological study

Viscosity measurements of selected formulations were assessed using parallel-plate rheometer (Anton Paar, Physica MCR 301, Germany). Shear rate was gradually increased from 0.01 to 600 S^{-1} and decreased again gradually at 25 °C and 35 °C. In addition, the measurements were carried by rising the temperature from 25 to 37 °C at a constant shearing rate of 300 S^{-1} to investigate the effect of temperature on viscosity.

2.13. Preparation of in situ gels incorporating FL nanodispersions

In situ gel formulations with optimum gelling capacities were selected to be medicated with FL. The final concentration of the drug was 0.3% (w/v). FL was incorporated in its plain form, niosomal vesicles or Eudragit nano-particles comprising the plain drug or its cyclodextrin complex. The pH of these formulations was determined, in triplicate, using pH meter (Thermo Fisher Scientific Inc., Orion VERSA STAR™, USA). The average reading was recorded.

2.14. In vitro drug release from the investigated formulations

Release profiles of FL were assessed using dialysis bag diffusion technique [47]. The profiles were estimated for the plain drug aqueous solution, selected situ gel formula, as well as *in situ* gels comprising the selected niosomal and Eudragit NPs formulations. The amount of tested samples equivalent to 3 mg drug was transferred into a presoaked cellulose dialysis bag (Dialysis tubing cellulose membrane, Sigma Co., USA; Molecular weight cutoff 12 000–14 000) and sealed at both ends. The bags were then immersed in well closed glass bottles, filled with 50 ml STF (pH = 7.4) as the release medium. The bottles were maintained at 35 ± 0.5 °C with a rotating speed of 50 rpm, using a thermo-stated shaking water bath (Memmert, SV 1422, Germany). At different determined time intervals, samples were withdrawn from the release medium and replaced with equivalent volume of fresh medium. The collected samples were analyzed spectrophotometrically at 261 nm using Shimadzu UV spectrophotometer (2401/PC, Japan). The cumulative percentage drug release versus time curves were plotted [47]. The experiment was done in triplicate and data were presented as the mean ± SD. The data of *in vitro* drug release were analyzed kinetically to assess the mechanism of FL release from the investigated formulae. Linear regression analysis for the release data was done, to determine the release model. Release model having R^2 value close to one was considered as best fit model. The data were fitted with different kinetic equations, zero order (cumulative drug released vs. time), first order (log cumulative drug retained vs. time), Higuchi model (cumulative drug released vs. square root of time) [48] and Peppas exponential equation (log cumulative drug released vs. log time), where values up to 60% of the release data are considered [49]. In Peppas model, the release exponent "*n*" was calculated which is indicative of drug release mechanism. The model affords a good explanation of the mechanisms governing the release. According to Peppas model interpretation, when $n = 0.43$ it indicates that the drug release follows Fickian diffusion mechanism. When the value falls in the range $0.43 < n < 0.85$ this indicates anomalous (non-Fickian) diffusion. A value of $n = 0.85$ indicates case II transport and a value of $n > 0.85$ indicates super-case II transport [50].

The area under the curve values from 0 to 8 h ($AUC_{0\text{-}8h}$) as well as the $AUC_{0\text{-}24}$ values for the cumulative percent drug released versus time curve were estimated using trapezoidal rule method. The mean time of drug release was calculated numerically as follows:

$$MRT = \sum_{j=1}^{n} \bar{t}\ \Delta Mj \Big/ \sum_{j=1}^{n} \Delta Mj$$

Where, j is the sample number, n is the number of sample times, ΔMj is the additional amount of drug released between t_j and t_{j-1}. $\bar{t}$ is the midpoint of the time period in which the drug fraction ΔMj has been released [51,52].

2.15. Ex vivo corneal permeability

Ex vivo corneal permeability study was performed using freshly excised rabbit corneas. The plain FL aqueous solution and the selected formulations comprising an amount equivalent to 1.5 mg drug were investigated. The study was conducted using Franz cell. The excised rabbit cornea was mounted between the donor and the receptor compartments so that the corneal epithelial surface was

facing the donor compartment with an exposed diffusion area of 0.5 cm^2, maintained at a constant temperature (35 ± 1 °C) and mounted on a magnetic stirrer adjusted at 100 rpm [19]. The selected formulations were placed on the corneal surface in the donor compartment and the receptor medium was 35 ml freshly prepared pH 7.4 isotonic phosphate buffer . Aliquots of the receptor medium were withdrawn after fixed time intervals from the sampling port and were replaced with equal quantity of fresh medium to maintain a constant volume. Samples were analyzed spectrophotometrically at 261 nm. Each formulation was evaluated in triplicate. The permeation parameters such as flux (*J*), permeability coefficient (*P*) were calculated for each formula. The flux (μg/cm^2 h) was calculated from the slope of the plot of the cumulative amount of drug permeated per cm^2 of rabbit cornea at steady state against time using linear regression analysis.

$$P = (dQ/dt)/AC = J/C$$

where: dQ/dt is the permeation rate at steady state of the cumulative flux curve, *A* is the surface area of the diffusion membrane, *J* is the slope of linear line of the plot and *C* is the concentration of the drug in the donor compartment [53]. Also, the *AUC* of the drug permeated through the cornea versus time was also calculated for each tested formula.

The results were expressed as mean ± SD. Statistical data were analyzed by one-way analysis of variance (ANOVA), and comparisons were made with post-hoc LSD test, using the SPSS software (version 22.0; IBM Co., USA).

2.16. *In vivo studies*

2.16.1. *Animals*

Male albino rabbits, weighing 2–2.5 kg were used in this study. All animals were healthy and free of clinically observed abnormalities. All eyes were initially examined and animals without any sign of ocular inflammation were included in the study. The studies were conducted in full compliance with local, national, ethical and regulatory principles for animal care and were approved by the National Research Centre Ethics and Animal Care Committee. The animals were kept in individual cages under well-defined and standardized conditions (humidity and temperature controlled room; 12-h light and 12-h dark cycle).

2.16.2. *In vivo eye tolerance test (modified Draize test)*

The rabbits were randomly divided into two groups, each group comprised three rabbits. Group A received the selected *in situ* gel comprising selected optimized FL niosomal formulation; Group B received the *in situ* gel comprising selected optimized FL Eudragit nano-particulate formulation. The application was always in the right eye of the rabbits and the left eye was used as the control and received no treatment. One drop 50 μl of each of the investigated formulations was instilled in the cul-de-sac of the right eye of each animal every 30 min for a 6-h period. This procedure was used to evaluate the safety for long-term therapy [54]. Eyes were visually examined at 1, 2, 4, 6, 24, 48 and 72 h after instillation for any irritation. A score for erythema was given as follows: 0, no reaction; 1, weak spotty or diffuse erythema; 2, weak but perceptible erythema covering the total eye area; 3, moderate erythema; 4, severe erythema with edema; 5, very severe erythema with defects.

2.17. *Histopathology*

For histological evaluation the same procedure adopted in the tolerance test except for that animals were euthanized after 2 h of the last instillation of the tested formulations. Subsequently the eye balls were carefully enucleated and washed with physiological saline. Corneas with marginal corneo-scleral junction (limbal area) were carefully dissected and stored in 10% formalin. Then washed with water and dehydrated with gradient concentrations of alcohol then inserted in warm molten paraffin and solidified in the form of blocks. Then corneal tissue was sectioned into 5 μm using a microtome. Then tissue sections were mounted on glass slides, de-paraffinized, stained by hematoxylin and eosin stain for examination through the light electric microscope [55].

2.18. *Corneal visualization using confocal laser scanning microscopy*

Observing the penetration of fluorescently-labeled tested *in situ* gel nano-formulation systems within the corneal tissue was performed by CLSM (ZEISS Co., Carl Zeiss, LSM 710, Jena, Germany). The used software was version: ZEN 2009. RhB was selected to simulate the drug. Rh B was used at a concentration of 0.3% (w/v) similar to the used FL concentration. Rh B-loaded niosomal vesicles and Rh B-loaded Eudragit NPs were prepared using the same procedures employed for preparing selected fluconazole-loaded nano-dispersions (FL-Nios and FL-ERS1) without cyclodextrin complexation and then embedded in the selected *in situ* gel (ISG3). In addition, Rh B aqueous solution, was investigated for comparison. One drop (50 μl) of each tested formulation was instilled once in the cul-de-sac of the rabbits eyes. Then, after 2 h the rabbits were euthanized and the whole eye balls were enucleated and washed with saline and the corneas with the surrounding limbal area were carefully dissected. Tissue sections of 5 μm thickness was prepared by the same procedure mentioned under the histopathological section, except that the tissue sections were not further processed or stained. The corneal tissue was mounted on glass slides and fluorescence was examined under microscope at an optical excitation of (λ_{ex} = 488 nm) argon laser beam and fluorescence emission was detected at (λ_{em} = 633 nm) [55].

2.19. *In vivo susceptibility test*

Candida Albicans NRRL Y-477 was chosen as a test organism to be used as a challenging yeast in the experiment as it is a well characterized and highly invasive strain that has been investigated in rabbit fungal keratitis model. Test tubes containing 5 ml of Muller Milton broth medium (MMB) were inoculated with 100 μl of *Candida* suspension containing 1×10^6 CFU/ml.

The rabbits were randomly divided into three groups, each group comprised six rabbits. Group A received 0.3% FL aqueous solution; Group B received the selected *in situ* gel comprising the selected drug niosomal formulation; Group C received the *in situ* gel comprising the selected Eudragit nanoparticulate formulation. All tested formulations comprised the same equivalent drug concentration. All solutions used in preparing the investigated nano-formulations and *in situ* gel were sterilized by filtration through sterile 0.22 μm pore size pyrogen-free cellulose filters and the preparation process was done under aseptic conditions [55]. Sterile 6 mm diameter filter paper discs (Whatman no. 1) were placed in the cul-de-sac of rabbit for 1 min at specific time intervals (1–24 h) following a single installation (50 μl) of the investigated formulae in the cul-de-sac of the right eyes of the rabbits. The discs were then placed in the nutrient broth (NB) tubes inoculated with 100 μl of bacterial suspension. The inoculated broth was then incubated at 37 ± 0.5 °C for 24 h. The growth inhibition of bacteria was evaluated by measuring the cultures optical density at 600 nm using a Shimadzu UV spectrophotometer (2401/PC, Japan). Percentage of inhibition, which is related to the level of drug in the eye tears following the topical application of tested drug formulae, was calculated using MMB inoculated with *Candida albicans* NRRL Y-477 as control.

The results were expressed as mean ± SD. Statistical data were analyzed by ANOVA, and comparisons were made with post-hoc LSD test, using the SPSS software (version 22.0; IBM Co., USA).

3. Results and discussion

Eudragit RL100 and Eudragit RS100 have been accepted to be used as controlled drug delivery excipients by the USFDA. They are proficient in forming small particle sized nano-dispersions. Their positive charge provide the bioadhesive character. This is attributed to their capability of interacting with the negatively charged mucosal layer covering the eye surface [47].

3.1. *Preparation of FL loaded niosomes*

The non ionic surfactant span 60 was more preferred than other non ionic surfactants in formulating niosomes with high entrapment values. This is related to its high phase transition temperature, the long saturated alkyl chain (C_{18}) and the optimum HLB. Also, cholesterol was used to improve stability and reduce leakage by reducing gel to liquid transition. Span 60 and cholesterol were used at 2:1 molar ratio to formulate the FL loaded niosomal vesicles (FL-Nios). FL-Nios have revealed adequate properties as depicted in Table 1. EE% was adequate reaching 67.4%. Particle size was 209.0 ± 35 nm. FL-Nios exhibited negative zeta potential which was equal to −36.0 ± 4 mV. It was high enough to maintain adequate stability. The negative charge was attributed to the existence of free carboxyl groups in surfactant and cholesterol molecules and also, the presence of hydroxyl ions which are adsorbed preferentially on niosomal vesicles surface.

It has been reported that niosomes prepared using Span 60: cholesterol at molar ratio 2:1 exhibited good properties. Increased surfactant amount can result in increasing the number of niosomal vesicles. Thus, more dug can be entrapped inside these vesicles. [44]. On the other hand, increased amounts of cholesterol can increase the vesicular membrane rigidity which may decrease the entrapment efficiency. Also, the use of further higher amounts of cholesterol may result in disrupting the layers order of niosomal vesicles [19].

3.2. *Preparation of FL loaded Eudragit NPs*

Eudragit RS100 and RL100 polymers were used to formulate positively charged FL NPs. These polymers are capable of forming, highly stable, positively charged nanosized dispersions. Their nanosized dispersions have been proven to be stable and safe. They also have been reported to be free from irritant effects on ocular tissue and capable of enhancing ocular permeability [56].

FL loaded Eudragit NPs were prepared using solvent displacement method. This method is simple and applicable for NPs preparation. The choice of the organic phase is of great importance for successful loading of the drug in Eudragit NPs. The selected organic solvent should have good water miscibility and high capability to dissolve both the drug and the polymer simultaneously. It should also have low boiling point to be easily evaporated [57]. In this study, acetone–methanol co-solvelent mixture was suitable to prepare the NPs. The solubility of FL in acetone is 4% (w/v) at 25 °C and it is freely soluble in methanol (25%, w/v). On the other hand, FL is only sparingly soluble in ethanol (2.5%, w/v), so this solvent was excluded [58]. Moreover, an inverse correlation has been reported between the dielectric constant and particle size. Methanol has high dielectric constant,thus, it can facilitate the formation of NPs with small particle size. The used ratio of organic to aqueous phase applied was 1:3. The mechanism of NPs formation involves spontaneous diffusion and flow between the interface of the organic and aqueous un-equilibrated phases. It has been reported that using larger volume aqueous phase in relation to the organic phase could result in increasing the diffusion of the water miscible organic phase into the aqueous phase thus assist small particle size formation. This may be attributed to that when the aqueous phase volume is increased, the formed NPs can move freely in the medium, with less chance of collision with each other, thus they can maintain their small size. On the contrary, the use of less aqueous phase would result in obtaining larger particle size particles [57]. Also, the water soluble surfactant PVA was used to enhance the physical stability and minimize the fast aggregation of formed NPs [59].

3.3. *Factorial design analysis of formulations variables*

Table 1 and Fig. 1 demonstrate the different compositions of the investigated formulations, their corresponding particle size and EE%. A full factorial design $2^1 \times 3^1$ was employed for developing and optimizing the investigated FL loaded Eudragit NPs. Table 2 depicts the effect of the independent variables on

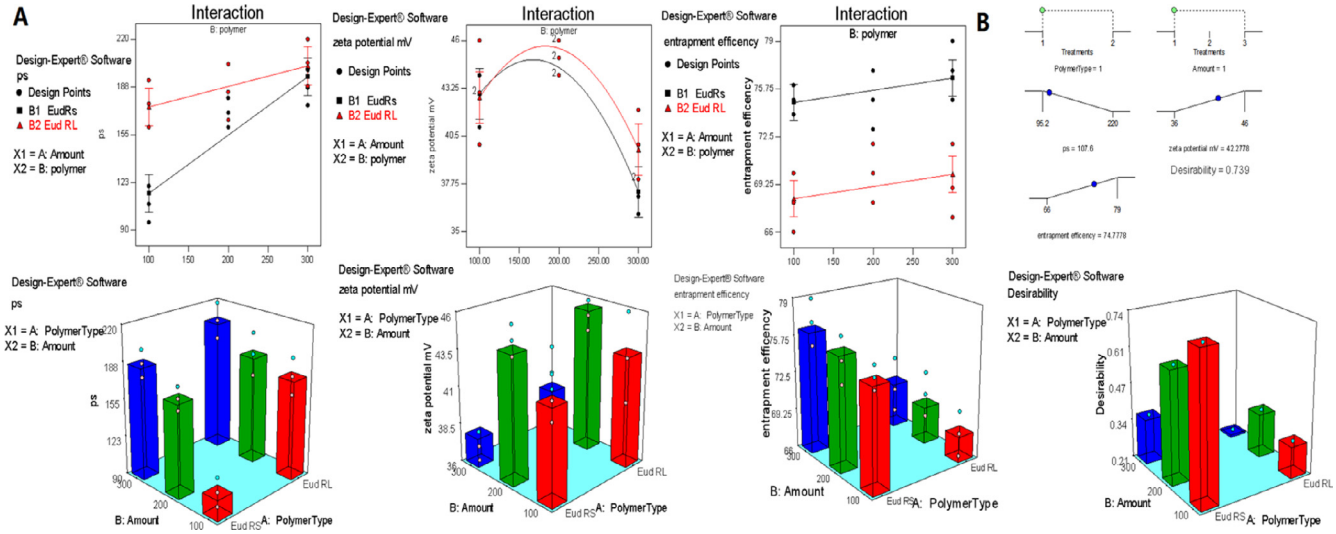

Fig. 1 – (A) Effect of independent factors (polymer type and amount) on the particle size, zeta potential and entrapment efficiency of the investigated FL-Eudragit nanoparticles. (B) The optimized selected formulation based on the desirability.

Table 3 – Output data of the full factorial design of fluconazole loaded Eudragit RS100 and Eudragit RL100 nanoparticles.

Response	Partical size (Y1)	Zeta potential (Y2)	EE% (Y3)
Suggested model	2FI	Quadratic	Linear
Model *F*-value	19.94	11.73	28.79
P-value prob > *F*	<0.0001	0.0003	<0.0001
Significant model terms	A, B, AB	(B, B^2)	A
(P-values)	(0.0007, <0.0001, 0.0154)	(0.0008, 0.0003)	(<0.0001)
Final equation in terms of coded factors	$+171.43+16.57\times A+26.85\times B-12.85\times A\times B$	$+45.00+0.56\times A-2.17\times B+0.67\times A\times B-4.33\times B2$	$+72.39-3.28\times A+0.83\times B$
R^2	0.8104	0.7830	0.7933
Adjusted R^2	0.7697	0.7162	0.7658
Predicted R^2	0.6926	0.5636	0.7028
Adequate precision	11.417	9.017	10.76

A: polymer type, B: polymer amount (mg).

particle size, zeta potential and EE%. The results revealed that the models were significant (Table 3). In addition, they were found to be good fitting; the"Pred *R*-Squared" were in sensible conformity with the "Adj *R*-Squared". Thus, the suggested models can be used to pilot the design method.

3.3.1. *Effect of formulation variables on particle size*

ANOVA test revealed that the particle size was significantly affected by the investigated factors. Also, the two factor interaction model (2FI) revealed that both the polymer type, its amount and their interaction were significant model terms. The "Prob > *F*" values were less than 0.05. It was noticeable that the use of equivalent amount Eudragit RL100 resulted in formation of particles with relatively larger size in comparison to formulations prepared by Eudragit RS100. This can be attributed to the increasing hydrophilicity provided by the quaternary amino groups. Eudragit RL100 has bigger percent of quaternary amino groups that results in increased hydration and swelling, hence resulted in larger particle size. Also, it was noticed that increasing the polymer amount, from 100 to 300 mg, was accompanied by the increasing particle size. Particle size of FLERS1 was 107.6 ± 12 nm, while FLERS3 increased to 187.4 ± 1 nm. Also, similar pattern was detected when Eudragit RL was employed. The corresponding particle sizes of FLERL1 and FLERL3 were 176.6 ± 21 and 234 ± 16 nm, respectively. This can be attributed to that higher polymer amount increased the viscosity of organic phase. It is assumed that more viscous organic phase affords higher resistance to mass transfer. Consequently, the polymer-solvent phase diffusion is reduced and bigger NPs are formed. On the contrary, decreasing the organic phase viscosity increases the distribution efficiency of the polymer-solvent phase into the external phase which lead to the formation of smaller NPs [57]. The results also revealed that PDI ranged between 0.27 and 0.55 was acceptable.

3.3.2. *Effect of formulation variables on zeta potential*

Aquadratic model was suggested when evaluating the zeta potential. The terms B and B^2 were significant. This reflected that the used polymer amount affected the magnitude of the surface charge significantly. A parbolic pattern for the zeta potential was noticed. The zeta potential values increased

Table 4 – Observed and predicted responses of selected optimized nanoparticles formula (FLERS1), mean ± SD.

Response	Observed values	Predicted values
Y1: particle size (nm)	107.6 ± 12	115.18
Y2: zeta potential (mV)	44.1 ± 2	42.95
Y3:EE%	75.3 ± 2	74.83

by increasing the polymer amount up to a certain limit afterwards it decreased. This may be attributed to that larger size particles are accompanied by less surface charge density which also tend to aggregate. The Eudragit NPs displayed positive zeta potential values which is attributed to the positive surface charge of the quaternary ammonium groups in the cationic structure of Eudragit RS100 and RL100. The positive surface charge is a favorable property of NPs intended for ophthalmic drug delivery system. It contributes in imparting mucoadhesion of NPs onto the eye corneal surface [57]. Positive surface charge of NPs can permit longer drug residence time on the eye surface *via* the interaction of the NPs with corneal and conjunctival glycoproteins. Thus, these NPs can act as depot to maintain prolonged effect [56,57]. Also, it was observed that the zeta potential values of Eudragit RL100 NPs were higher than Eudragit RS values. This may be attributed to the higher content of the positively charged quaternary amino groups in relation to Eudragit RS100.

3.3.3. *Effect of formulation variables on the EE%*

A linear model for EE% was suggested where the type of the polymer was the significant term. The polymer type played a pivotal role in governing the entrapment efficiency of the formulations. Eudragit RS100 can form compacted wall particles with less porosity. These properties can contribute in decreasing drug leakage. This is attributed to its less hydrophilic nature in comparison to Eudragit RL100.

3.3.4. *Optimization and validation of the investigated FL loaded Eudragit NPs*

Optimization of pharmaceutical dosage formulations is generally carried to determine the compromised level of variables that could attain best required outcomes. In this study the desirable criteria were to mimize particle size (Y1) and maximize both zeta potential magnitude and EE% (Y2 and Y3). The optimum levels of the independent variables based on the desirable criteria constrains were suggested by graphical and numerical analysis using the Design-Expert software.

The evaluation revealed that the optimized FL-Eudragit NPs with the highest desirability comprised Eudragit RS100 at a drug to polymer ratio of 1:4 Thus, the suggested formula was FLERS1. Table 4 presents the observed and predicted values for FLERS1. The results revealed that the observed values were closely similar to the predicted values. This confirmed the method reliability. Based on the obtained results, it can be concluded that the optimized formulation could provide an adequate promising platform for further manipulation.

3.4. *Preparation of Eudragit NPs and niosomal vesicles incorporating FL in the form of FL-HP-β-CD complex*

The second step of this study was to elucidate the impact of incorporating FL-FL-HP-β-CD inclusion complex in the prepared niosomal formula and the selected optimized formula FLERS1.

The structure of the Fl-HP- β-CD inclusion complex was studied by Li et al. using ^{1}H NMR and powder X-ray diffraction spectra [41]. They indicated that the complexation disturbed the head-to-head channel type structure of HP-β-CD to form a new 1-D chain head-to-tail channel packing. The researchers proved, via phase solubility method, continuous variation fluorescence and ESI–MS analysis. that the stoichiometric ratio was 1:1. The evidence of forming a 1:1 stoichiometric ratio and its structure conformation of complex formation depended on the cylodextrin cavity size, van der Waals forces, hydrophobic interactions and hydrogen bonding. The inner diameters of β-CD hydrophobic cavity were 0.60 nm in the narrower end and 0.68 nm in the wider end, respectively. While in FL molecule, the longest distance between different atoms of triazolyl and fluorinated phenyl rings were reported to be 0.41 and 0.62 nm using the crystal data. According to the size matching rule, the inclusion complex structure suggested that a triazolyl ring of FL was entrapped into the narrower end of the cavity and the 2,4-difluorophenyl ring into the wider end. This resulted in the formation of a complex at a 1:1 stoichiometric ratio with the head-to-tail packing. In addition, the three sp3 carbon atoms linking two triazolyl rings afforded good flexibility and decreased the steric hindrance, the hydroxyl proton of the central carbon and triazolyl nitrogen atoms of FL promoted the hydrogen bonding with the cyclodextrin. Moreover, the hydroxypropyl group in HP-β-CD was believed to promote in the hydrogen bonding interaction to generate a stable inclusion complex [41].

When employing cyclodextrn in drug delivery systems, it is important to use just the adequate amount of the cyclodextrin without any excess to form the complex. This is contributed to that the drug absorption enhancement is only achieved when just an adequate amount of cyclodextrin is used in the preparation. Using adequate amount of cyclodextrin will maintain the thermodynamic activity of the drug molecules to be equal to unity in the tear fluid. In turn, the dissolved drug will be at its highest potential. Consequently, this will result in increasing the solubility of drug in tear fluid and enhancing the permeation through ocular membranes. Thus, this can contribute in solving major problems such as the poor aqueous solubility and low ocular permeability of topical ophthalmic drug delivery [26]. Accordingly, FL-HP-β-CD inclusion complex was prepared by the kneading method at a 1:1 molar stochiometric ratio. The selected optimized Eudragit nanoparticles formula (FLERS1) in addition to the niosomal vesicles formula (FL-Nios) were prepared incorporating the equivalent of the drug FL in the form of FL-HP-β-CD complex. The obtained niosomes were further coated with chitosan. Coating NPs with chitosan has gained interest as it can impart bioadhesive characters to the particles, enhance their interaction with mucin layer on the

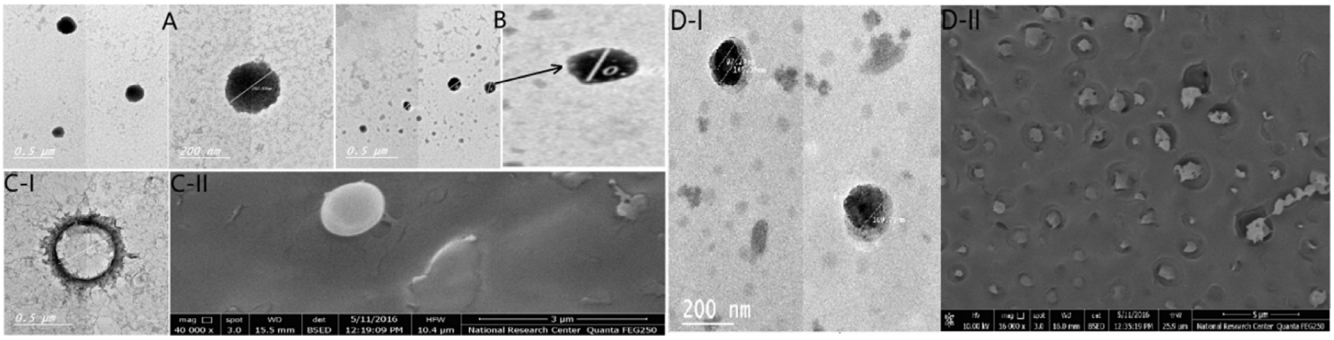

Fig. 2 – TEM micrographs of FL-Nios formula (A), FL-ERS1 (B), FL-CD-Nios1 (C-I) and FL-CD-ERS1 (D-I) and SEM of FL-CD-Nios-Ch (C-II) and FL-CD-ERS1 (D-II).

eye surface and increase drug local concentration [44]. Two types of interactions contribute in this phenomenon. The first type is the electrostatic interaction between the acidic sialic residues of mucin and the amino groups on the polycation polymer chitoson. The second is the hydrophobic interaction due to methyl groups on chitosan acetyclated residues and methyl groups that lie on the side chains of mucin [44].

3.5. *Characterization of selected prepared niosomal and Eudragit NPs*

3.5.1. *Estimation of the particle size, zeta potential and EE%*

The particle size was estimated for the optimized chitosan coated niosomal vesicles that comprised FL-HP-β-CD complex (FL-CD-Nios-Ch). The investigations revealed that particle size was 392.8 ± 27 nm; PDI was 0.74; zeta potential was 28.5 ± 5 mV and EE% was 61.7%. The increment in the particle size was attributed to the thickness of the chitosan coating. Moreover, this coat lead to reversing the zeta potential charge sign from –ve charge of the uncoated niosomal vesicles to +ve charge.This positive charge can share in imparting prolonged contact time between the drug, corneal and conjunctiva tissue. This is attributed to the ionic interaction with the negatively charged sialic acid residues of the mucin on eye surface. However, the entrapment efficiency was not significantly affected. Regarding Eudragit RS100 NPs comprising FL-HP-β-CD complex FL-CD-ERS1 the estimated particle size was 151.1 ± 19 nm, PDI was 0.38; the zeta potential was 40.1 ± 3 mV and EE% was 76.4%. This reflects that entrapping the drug in the form of cyclodextrin complex lead to an increase in the particle size of the formed NPs. Similar results have been reported by other researchers [34,60]. Also, the results depicted maintenance of the adequate +ve zeta potential. This reflects that appropriate stability was reserved. These results are in accordance to other studies which reported that zeta potential values were not much affected by entrapping the drug as a cyclodextrin complex [60,61]. Also, EE% did not differ much in comparison to the conventional ones. However, some results reported by other researchers regarding the difference in EE% were contradictory and were dependent on the drug properties and the preparation techniques of the nanocarriers [34,35].

3.5.2. *Morphological study using transmission electron microscopy and scanning electron microscopy*

Fig. 2 reveals the morphology of selected NPs namely FL-Nios, FL-ERS1, FL-CD-Nios-Ch and FL-CD-ERS1. The morphology was examined by TEM and SEM. The photomicrographs show that the NPs were distinct, spherical with smooth surface without aggregations. It was evident that drug encapsulation in the form of cyclodextrin lead to size increments in comparison to the conventional investigated Eudragit NPs and niosomal vesicles. Also, chitosan coating of the niosomes was evident. It is worthy to mention that the increment in the particle size was acceptable as it remained in the nano range. Moreover, SEM clarifies that the investigated particles have spherical shapes without aggregations.

3.5.3. *FTIR and X-ray diffractometry*

The prepared nano-formulations were characterized using FTIR. Fig. 3 illustrates the IR spectra of FL and the investigated formuatons. FL spectrum presented several distinctive bands. A broadband appears at 3400 cm^{-1} due to hydrogen bonding O–H stretching vibration. The bands that fall in the range of 3120–3070 cm^{-1} are related to aromatic stretching vibration. Overtone and combination bands correspond to 1.2,4-tri-substitution of the phenyl group appear at 1770, 1845 and 1900 cm^{-1}. The bands that appear at 1620, 1600, 1520 cm^{-1} correspond to aromatic C–C and C–N stretching vibration. Bands appearing at 1220 and 1210 cm^{-1} are due to aromatic C–F stretching vibration. The band at 1150 cm^{-1} is consistent with tertiary alcohol stretching vibration. The band appearing at 850 cm^{-1} is due to the out of plane C–H deformation vibration of two adjacent aromatic hydrogen atoms.

The IR spectra of FL-HP-β-CD complex showed broad band between 3000 and 3400 cm^{-1} region related to O–H stretching vibration and the bands in the range of 2920 to 3000 cm^{-1}. These bands are due to CH and CH_2 stretching vibrations. The O–H bending at nearly 1600 cm^{-1} and C–H bending at 1160 cm^{-1}. The IR of the prepared FL-HP-β-CD complex showed clear alterations in comparison to the drug. There were detectable reduction of several peaks intensities, bands shifting, and disappearance of some peaks suggesting the hydrogen bonding and the host guest interaction due to inclusion complexation of FL within the cyclodextrin cavity.

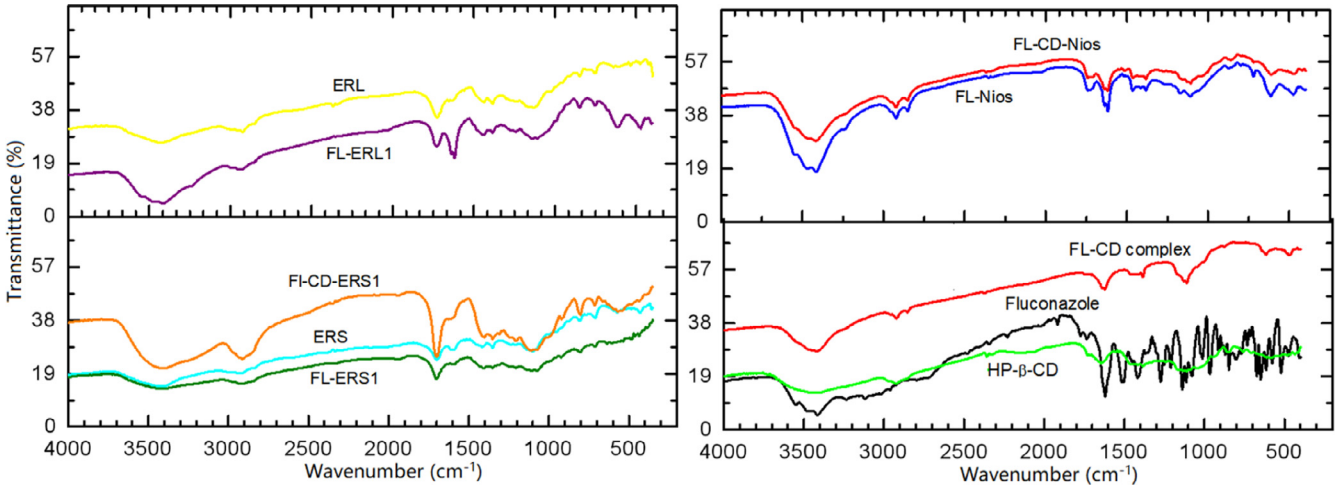

Fig. 3 – FTIR spectra of fluconazole, HP-β-CD, FL-CD-HP-β-CD complex, Eudragit RS100, Eudragit RL100 and selected investigated fluconazole loaded formulations.

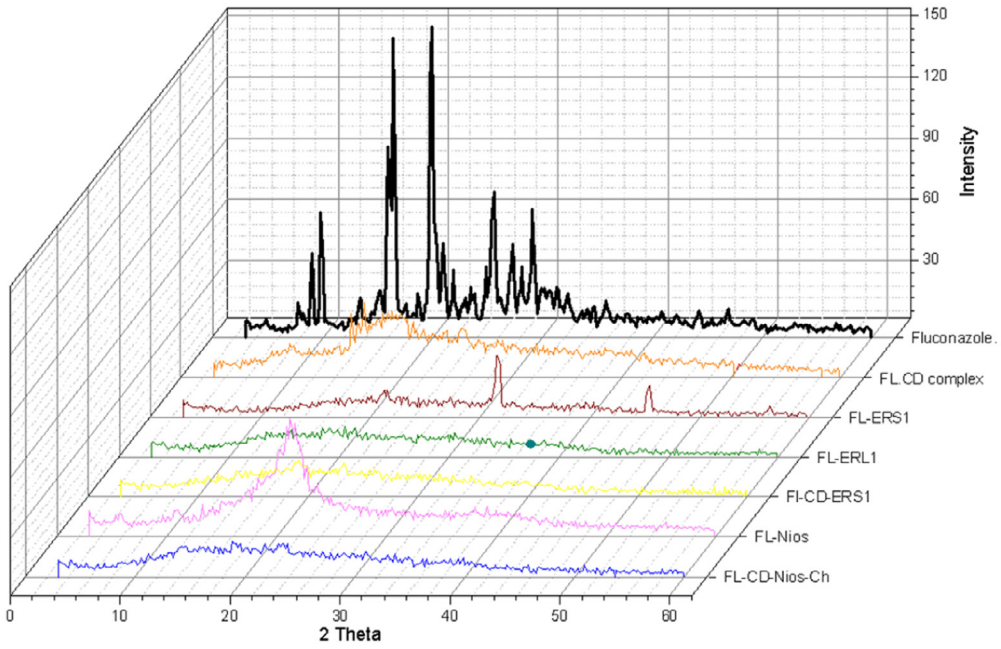

Fig. 4 – X-ray diffraction pattern of fluconazole, FL-CD-HP-β-CD complex, Eudragit RS100, and selected investigated fluconazole loaded formulations.

Bands shifting, reduction of their intensity, disappearance of some bands can be related to changing to an amorphous structure [43]. The IR spectra of Eudragit RS100 displayed characteristic bands due to the ester groups in the range of 1240–1130 cm^{-1}. Also, a band appeared at 1727 cm^{-1} related to C=O stretching vibration. Moreover, CH vibrations bands were distinguished at 1380 cm^{-1}, 1450 cm^{-1} and in the range between 2900 and 3000 cm^{-1}. Eudragit RL 100 displayed IR absorption bands at 3300 cm^{-1}, 2800 cm^{-1}, 1700 cm^{-1} and 1600 cm^{-1}. These bands corresponds to OH stretching, CH stretching, C=O stretching and presence quaternary ammonium group, respectively.

The encapsulation of drug- either in its plain form or as a cyclodextrin complex in the niosomal vesicle or Eudragit NPs lead to detectable shifting and broadening of several bands. These changes were remarkable in the region of 3400 cm^{-1}. This band is related to O–H stretching vibration. This could be due to involvement in hydrogen bonding. Also, changes were observed for bands in the region from 1200–1900 cm^{-1}. These changes were assigned to O–H bending and C–H bending.

Fig. 4 shows the X-ray diffraction patterns of selected formulations. X-ray diffraction pattern of FL plain drug powder depicted sharp intense peaks at 2θ values = 19.96, 19.44, 16.44, 19.8, 25.56,16.6, 16.2 and 9.08. These sharp intense peaks indicated the crystalline state. However, the diffraction pattern of drug cyclodextrin and the investigated formulations showed halo-pattern of diffraction. The diffraction peaks appeared diffused broad and of low

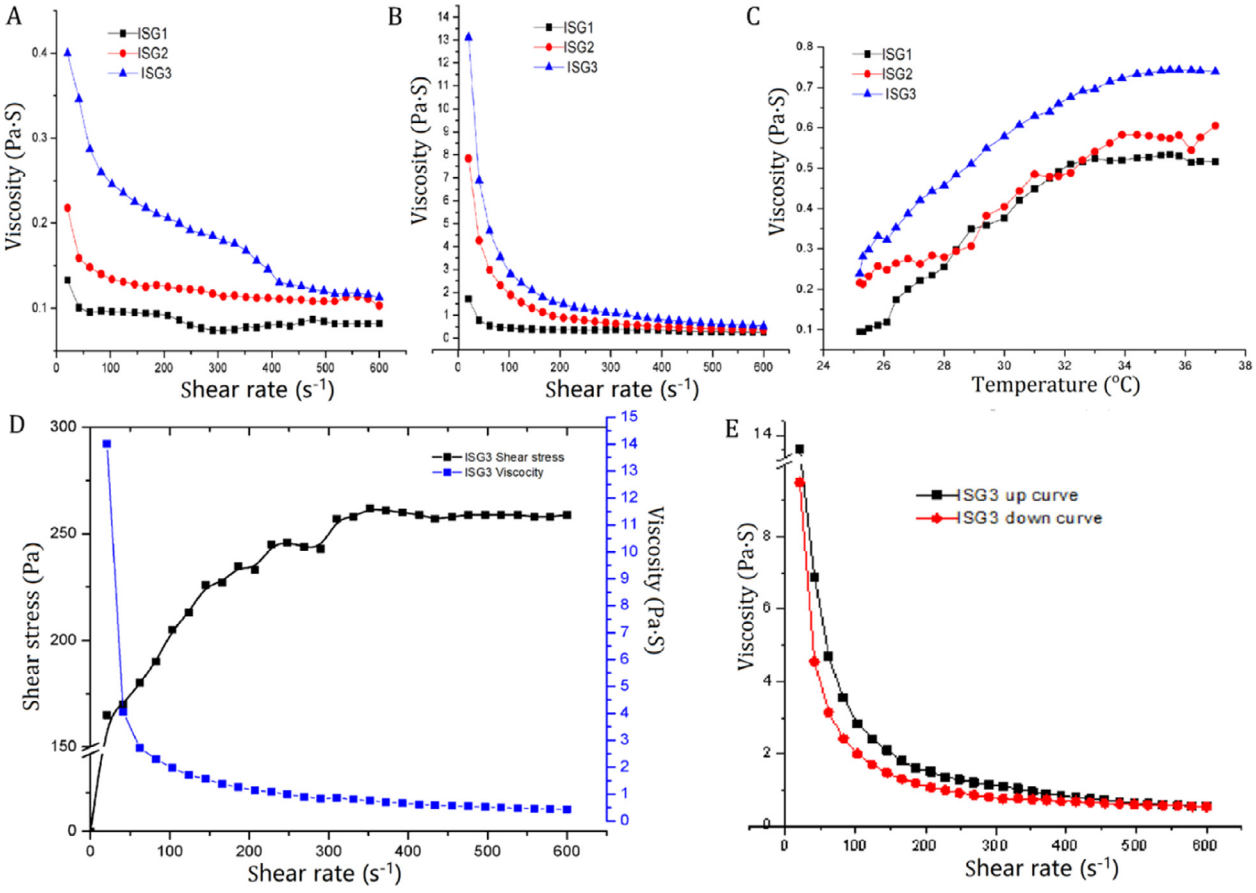

Fig. 5 – Rheograms of different investigated *in situ* gelling formulations displaying shear rate versus viscosity at 25 °C (A) and at 35 °C (B); viscosity at the temperature range between 25 and 37 °C (C); shear rate versus shear stress (D); up and down curve of the selected *in situ* gelling formulations (E) .

intensities. This suggests the change from the crystalline state to amorphous state with smaller particle size. The crystallinity could be determined by comparing some representative peak heights in the diffraction patterns of the complex with those of a reference. Which is comparing the peak height of the sample to that of the peak height of the reference appearing with the highest intensity at the same angle. The relative degree of crystallinity values were: 0.22, 0.23, 0.07, 0.095, 0.10 and 0.103 for FL-HP-β-CD complex, FL-Nios, FL-CD-Nios-Ch, FL-ERS1, FL-CD-ERS1 and FL-ERL1, respectively.

3.6. *Preparation of thermosenstive in situ gel*

Although nanocarries can enhance drug ocular absorption nonetheless the rapid tear turnover and nasolacrimal drainage contribute to big extent in decreasing topical ocular drug bioavailability. This prompted us – in the third step of optimizing the formulations – to incorporate the selected nano-formulations into *in situ* forming gel to manipulate this problem. *In situ* gelling formulations can be instilled in the eye easily in the form of drops and transferred spontaneously into a gel on the eye surface.

Poloxamers are synthetic amphiphilic copolymers consisting of a hydrophobic central block of polyoxypropylene oxide (PPO) surrounded by hydrophilic blocks of polyoxyethylene oxide (PEO). These polymers self assemble to form small micelles at low temperatures. When the temperature is increased these polymer transfer from liquid to semisolid. This is attributed to that when the temperature increases the PPO chains become less soluble and dehydrate. Also, confirmation changes occur at this hydrophobic region and spherical micelles are formed. These micelles aggregate and entangle which result in three-dimensional network. The unbound water becomes more available at the hydrophilic external region of the PEO which interpenetrate into the gel. At the gelling point the micelles are orderly packed and become intact like hard spheres. The internal core of these micelles are the hydrophobic PPO chains and the PEO chains are the external region.

In this study thermosensetive polymeric *in situ* gelling formulations comprising poloxamer 407 were prepared. This was based on its thermosenstive property and its good safety. Poloxamer 407 shows concentration and temperature dependent rheological properties. It is transferred into a gel at room temperature at concentration greater than 20%. Thus, it will not be free flowing and cannot be easily administered precisely in liquid eye drop form. On the other hand, Poloxamer 407 at concentrations less than 15% cannot form gel at physiological eye temperature [46,62]. Ideally, the

Table 5 – Compositions and physical characterizatin of the prepared *in situ* gels. Data represented as mean ± SD ($n = 3$).

In situ gel name	Composition	Gelling temperature	Gelling capacity	Farrow's constant
ISG1	18% Poloxamer	35.7 ± 0.2	++	2.6
ISG2	18% Poloxamer + 0.2% chitosan	35.4 ± 0.6	++	3.2
ISG3	18% Poloxamer + 0.2% chitosan + 1.5% HPMC	34.3 ± 0.5	++	3.3

system is expected to gel immediately or within a brief time upon exposure to its gelling temperature to prevent the quick washing out by tear turnover.

However, it was reported that poloxamers suffer from poor mechanical strength that leads to fast erosion [46,62]. Thus, different approaches were conducted to cope with this problem. These approaches were based on blending poloxamers with other polymers having bioadhesive properties like carbopol, chitosan, HPMC and alginate [63] Thus, we investigated the use of 18% concentration of plain poloxamer or blended with 0.2% chitosan and 1.5% HPMC for developing a suitable *in situ* gelling formula. The *in situ* gelling formulations of different compositions were prepared and their gelling capacities were evaluated to select the optimum formula (Table 5).

3.6.1. *Evaluation of rheological behavior of the investigated* in situ *gel formulations*

Fig. 5 illustrates the rheological behavior of the investigated *in situ* gelling formulations. Fig. 5A and 5B demonstrates the rheological behavior at ambient temperature and at eye physiological temperature 35 °C, respectively. The investigated formulations exhibited shear thinning pseudoplastic flow behavior at both room and physiological temperatures. The viscosity decreased as a consequence of increasing the shear rate. It can be clearly noticed that the viscosity values are much higher at 35 °C (Fig. 5B) in comparison to that measured at room temperature (Fig. 5A).

It was also depicted that the formula incorporating 0.2% chitosan (ISG2) showed higher viscosity values at all the investigated shear rates. Also, it was depicted that further incorporating 1.5% HPMC in addition to 0.2% chitosan (ISG3) lead to further enhancement in the viscosity values of the gel. This reflected the formation of a more firm net work structure. Farrow's index values were obtained by calculating the slope of log shear rate vs. log shear stress plot therapy [53]. The depicted values were greater than one. This confirmed a non Newtonian pseudoplastic flow behavior (Table 5). This type of flow is preferable as it interferes minimally with the tear fluid which also exhibits pseudoplastic type of flow.

Fig. 5C illustrates the impact of raising the temperature from 25 to 37 °C while subjecting the formulation to a constant shear rate on the viscosity of the *in situ* gelling formulations. As depicted all the investigated formulations revealed thermosenstive behavior and the viscosity increased with increasing the temperature. It was obvious that the blended gelling formula (ISG3), which comprised 18% poloxamer 407, 0.2% chitosan and 1.5% HPMC, demonstrated the highest viscosity values. The increase in viscosity was gradual at low temperature but the increment was more detectable at nearly 34 °C which is desired as it is nearly the precorneal temperature.

Fig. 5E illustrates the up and down curve of ISG3 which showed that by increasing the shear rate the viscosity decreased. The gradual decrease of shear stress resulted in increasing viscosity once more and reforming the structured network gel structure. Also, a hystress loop was depicted between the up and down curves. This is an indication of thixotropy. *In situ* gel with such characteristics is regarded suitable. It can spread on the eye surface upon blinking then regain high viscosity at low shear rate during the inter blinking periods. Thus, it can maintain prolonged ocular residence time.

3.6.2. *Determination of gelling capacity and the sol–gel phase transition temperature of the prepared in situ*

Table 5 illustrates the gelling capacity of the formulations. It was revealed that the sol–gel transition temperature was not much affected by incorporating 0.2% chitosan. It has been reported that blending chitosan, at low concentrations with Poloxamer 407. could not much effect the sol–gel transition temperature. On the other hand, it could help in improving the gel mechanical properties. It could make it more tight and can modulate the diffusion coefficients inside the gel structure. It could also help in accommodating the unbound water that resulted from dehydrating the PPO micelle core. This could lead to more entanglements and could increase the elasticity of system network. In addition, chitosan could also be beneficial as it has mucoadehsive and penetration enhancing effects.

The supplementary incorporation of HPMC in the gel formula resulted in decreasing the gelling temperature to 34.3 °C, which is simillar to the corneal surface temperature. HPMC interacts through hydrogen bonding with polyoxyethylene chains of the poloxamer molecules. This binding initiates dehydration which results in promoting adjacent molecules entanglement. Hence, this causes the decrease in gelling temperature. Thus, the used blend of polymers in ISG3 formula was satisfactory to be used for topical ophthalmic administration. This mixture is liquid at room temperature and could transfer to gel immediately at physiological eye condition. Moreover, its high viscosity would help in withstanding the high shear rate values encounterd during blinking. It would help in decreasing the drug loss caused by the rapid tear turnover and drainage through the nasolacrimal duct. This would help in prolonging the contact time and would contribute in sustaining the drug effect.Thus, ISG3 formula was selected to be incorporated with the plain drug and nano-formulations. The gelling temperature and the pH of this formula were measured after blending the drug.

Table 6 – *In vitro* release studied parameters of fluconazole in the investigated formulations.

Formula	MDT	AUC_{0-8h}	AUC_{0-24h}	Best fitting release model	R^2	*n* exponent of peppas model
FL aqueous solution	2.11 ± 0.04	582.61 ± 4.9				
FL/ISG3	2.75 ± 0.06	505.54 ± 6.3	–	Higuchi	0.995	0.39
FLNios/ISG3	6.42 ± 0.13	335.83 ± 2.3	1716.2 ± 4.6	First	0.992	0.47
FL-CD-Nios/ISG3	6.78 ± 0.06	321.10 ± 2.1	1708.1 ± 2.7	First	0.990	0.45
FLERS1/ISG3	6.69 ± 0.19	322.70 ± 7.1	1711.6 ± 12.1	First	0.993	0.62
FL-CD-ERS1/ISG3	6.94 ± 0.08	314.12 ± 3.6	1704. 2 ± 8.6	First	0.989	0.58
FLERL1/ISG3	6.50 ± 0.11	330.82 ± 2.4	1726.3 ± 3.9	First	0.992	0.46

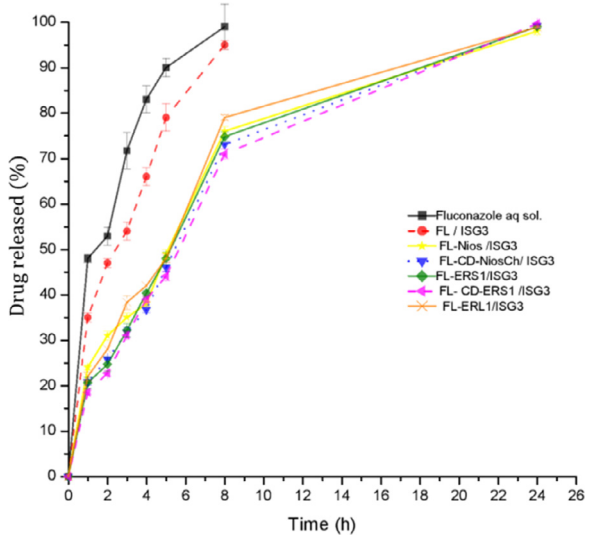

Fig. 6 – *In vitro* release profile of fluconazole from aqueous solution and the investigated selected formulations through cellulose membrane in simulated tear fluid at 35 °C.

It was revealed that the gelling temperature was not affected after drug loading. In addition, the measured pH was 6.5 ± 0.7 which is acceptable for topical ocular administration.

3.7. *In vitro drug release from the investigated formulations*

Table 6 and Fig. 6 illustrate the drug release pattern from the investigated formulations in simulated tear fluid at physiological eye temperature. The results revealed that the release pattern of the plain drug aqueous solution was the fastest. The MRT was significantly shorter than all other investigated formulations ($P < 0.05$). Incorporating the plain drug in the *in situ* gelling formula FL/ISG3 revealed sustained drug release pattern in comparison to the drug aqueous solution. It also led to a significant increase in the MRT ($P < 0.05$) in comparison to it. This may be attributed to that the net-work gel structure of ISG3 formula promoted controlled drug release and suppressed premature fast drug release. Moreover, it was detected that FL-Nios-ISG3, FLERS1/ISG3 and FLERL1/ISG3 exhibited significantly longer MRT ($P < 0.05$).

Eudragit RS100 and Eudragit RL are water insoluble. But, hydration of the formed NPs can lead to structure relaxation and pores formation through which the drug can diffuse in a controlled manner. It was also depicted that the release was faster and the MRT was significantly shorter for the FLERL1/ISG3 formula in comparison to FLERS1/ISG3. This can be attributed to the higher content of quaternary ammonium groups of Eudragit RL, in comparison to Eudragit RS100. These groups promote hydration and thus increase permeability of the NPs to the aqueous dissolution media. Thus, the drug can diffuse relatively faster.

It was also depicted that the coated niosomal formula (FL-CD-Nios-Ch/ISG3) and Eudragit formula (FL-CD-ERS1/ISG3) comprising the drug cyclodextrin complex showed further sustained effect. The MRT was longer by ~7.8% and ~4.6% in comparison to FL-Nios/ISG3 and FLERS1/ISG3 formulations, respectively. The difference was significant ($P < 0.05$). Nevertheless, the increase in the MRT was accompanied by a decrease in the cumulative drug released in the first period of drug release. $AUC_{0\text{-}8\,h}$ was significantly smaller. However, cumulative percentage drug released increased gradually in the second period of drug release. Thus, the difference in the $AUC_{0\text{-}24\,h}$ was not significant. The observed prolonged release pattern may be attributed to that the drug cyclodextrin complex was entrapped deeply within the core of the niosomal vesicles or Eudragit NPs. Thus, adequate time was required for hydrating these nano-systems to permit the external aqueous media to diffuse to the internalized hydrophilic drug-HP-β-cyclodextrin complex. The drug is released either in the form of intact cyclodextrin complex or in free dug form which exists in equilibrium with the complex [64]. The obtained results agree with other results reported in several studies which have also reported a more prolonged and sustained drug release from nanocarriers in which the drug was incorporated as a cyclodextrin complex in comparison to conventional nanocarriers [34,35,38,65–67]. On the other hand, fast release pattern results have also been reported by other researchers [61]. Chen et al. have reported that a fast release phase of drug could occur as a result of the presence of the drug within the outer shallow wall layers of the nanocarrier while slow release rate phase was contributed to that the entrapped drug was deeply internalized within the nanocarrier [64].

Cyclodextrin complexation have provided better performance regarding the intended prolonged release of the investigated optimized nano-formulations. The cyclodextrin complexation prevented the fast leakage of the drug from the conventional nano-carriers. This was

Table 7 – Permeabilty parameters for the selected formulations and Fluconazole aqueous solution through excised rabbits corneas. Data represented as mean ± SD ($n = 3$).

Formulation	Flux ($\mu g/cm^2/h^2$)	Permeability coefficient (cm/h)	$AUC_{0\text{-}6h}$ ($\mu g \cdot h/cm^2$)
FL aqueous solution	56.2 ± 3.7	0.019 ± 0.004	52.17 ± 5.6
FL-CD-Nios/ISG3	139.38 ± 14	0.046 ± 0.005	101.03 ± 5.9
FL-CD-ERS1/ISG3	189.9 ± 5.8	0.063 ± 0.002	123.06 ± 6.3

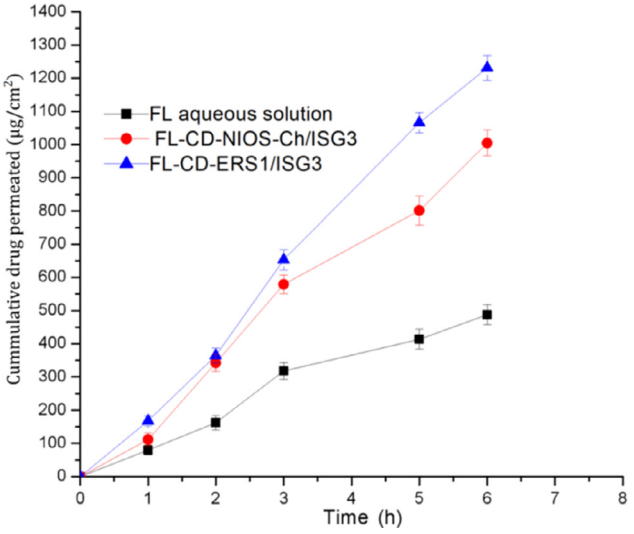

Fig. 7 – Ex *vivo* permeation profile of fluconazole aqueous solution, Fl-CD-NIOS/ISG3 and FL-CD-ERS1/ISG3 formulations through excised rabbits corneas at 35 °C.

attributed to the high drug affinity to the cyclodextrin. The free drug gradual release is governed by the stability constant of complex formation and the complex dissociation. In addition, cyclodextrin complexation could contribute in augmenting the nanocarrier performance by maintaining the drug solubilized at high concentration and providing high chemical potential which faciltate drug passage through membranes. Also, cyclodextrins can act as carriers which transport the drug to be in close proximity with membranes through which it permeate. In addition, cyclodextrin complexation could improve drug stability and prevent formulation incompatibilities [26,27]. Besides, cyclodextrin complexation could increase the tendency of cyclodextrins to self assemble and form new nano-aggregates which could contribute in more prolonged drug release patterns [68].

The kinetic order of FL release from the investigated formulations was studied. The drug release of *in situ* gel incorporating the plain drug was best fitted to Higuchi order. However, the release pattern of all other investigated formulations most fitted to first order pattern. Thus, the release pattern was concentration dependent. Fitting the release pattern to Peppas model revealed anomalous drug release pattern. The *n* values (the diffusional exponent) were in the range of $0.43 < n < 0.85$. This pattern is governed by more than one mechanism that may include drug diffusion, relaxation and erosion.

In conclusion, the *in vitro* release study depicted complete and prolonged drug release pattern from all the investigated nano-formulations. However, the formulations incorporating the drug as a cyclodextrin complex (FL-CD-Nios-Ch/ISG3 and FL-CD-ES1/ISG3) depicted more prolonged effect. Thus, these formulations were chosen for further investigation.

3.8. *Ex vivo corneal permeability*

Table 7 and Fig. 7 present the *ex vivo* permeation study through excised rabbit cornea. The obtained results revealed significant increase ($P < 0.05$) in the drug flux, permeation coefficient and the $AUC_{0\text{-}6\,h}$ of the investigated formulations in comparison to the plain drug solution. The steady state flux of FL-CD-Nios-Ch/ISG3 and FL-CD-ES1/ISG3 was nearly 2.5 and 3.4 times that of free drug aqueous solution, respectively. Likewise, $AUC_{0\text{-}6\,h}$ of these formulations was nearly 1.9 and 2.4 times that of the plain drug solution. Also, these investegigated parameters were significantly higher ($P < 0.05$) for FL-CD-ERS1/ISG3 formula in comparison to FL-CD-Nios-Ch/ISG3. The better performance of FL-CD-ERS1/ISG3 could be attributed to its smaller particle size (151.1 nm) and higher positive zeta potential value (40.1 mV) in comparison to FL-CD-Nios-Ch which revealed larger particle size (392.8 nm) and smaller zeta potential (28.5 mV). The particle size of the investigated Eudragit NPs was smaller than half that of the investigated niosomal vesicles. This would provide larger surface area available for drug permeation. Also, the higher positive zeta potential would promote better interaction between the Eudragit NPs and the negatively charged corneal surface. Thus, it would improve the formula bioadhesion, increase its residence time on the corneal surface and augment the drug permeation.

Enhanced permeation through biological membranes has also been reported when using nanocarriers comprising different drugs-cyclodextrin complexes [36,69–71]. Cyclodextrins act as penetration enhancers in ocular drug delivery *via* different mechanisms. It is also safe in comparison to other chemical enhancers. Cyclodextrins large molecules do not penetrate biological membranes but it keep the drug in a solubilized form at the surface of the membrane through which the free drug can be partitioned and permeate through biomembranes. It is known that drug-cyclodextrin complexes, dissociate to be in equilibrium with the free drug that can gain access into membranes. It has also been reported that in aqueous solution a drug cyclodextrin complex can self assemble to form nano-scale particles and aggregates. Thus, drug cyclodextrin complex molecules, dissolved drug molecules and drug-cyclodextrin self assembled NPs co-exist [26]. In aqueous media these nanodisperions account for several physicochemical properties and biological performance of the system [68]. It has been reported that topical ocular

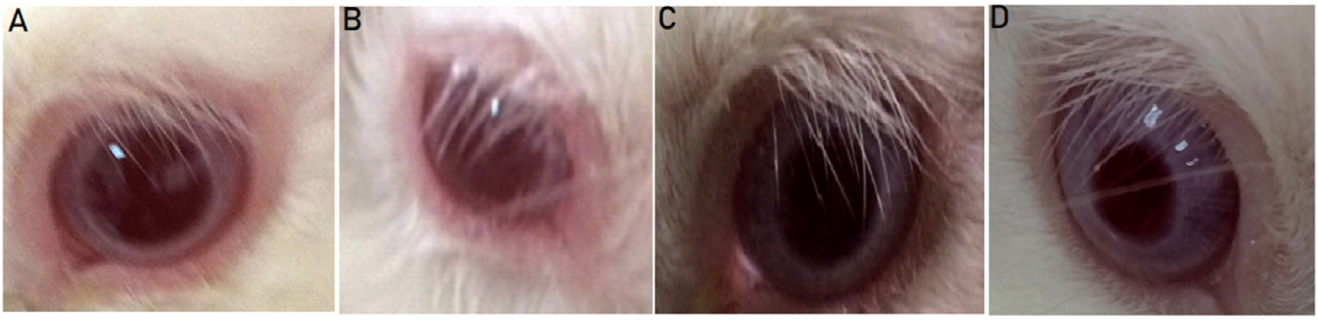

Fig. 8 – Ocular tolerance test for rabbits eye normal control eye (A); the eye that received FL-CD-Nios-CH/ISG3 (B); control eye (C); the eye that received FL-CD-ERS1/ISG3 (D).

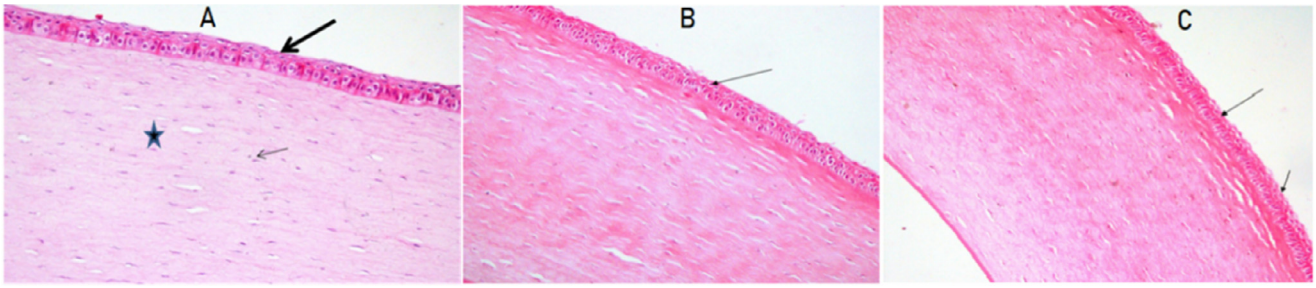

Fig. 9 – Photomicrography of the histopathological study of the examined rabbits corneas normal controI (A); group that received Fl-CD-NIOS/ ISG3 (B), group that received FL-CD-ERS1/ISG3 (C). Normal tissue architecture with normal lining epithelium (thick arrow), nuclei of corneal cells (thin arrow) and normal collagenous stromal lamellae (star). (H&E) x 200).

eye drops comprising cyclodextrin resulted in delivering significant amounts of the drug to both anterior and posterior eye segments. Moreover, clinical evaluations declared the possibility of replacing invasive ocular drug delivery routes such as intravitreal injections [26]. Nonetheless, when using low viscosity eye drops the drug-cyclodextrin complex systems can be washed out quickly before the free drug release. Thus, incorporating drug-cyclodextrin within a nanocarrier can act as a reservoir that can conquer the rapid wash out and drug loss [72]. Furthermore, blending the proposed systems in an *in situ* gel could have shared in augmenting the drug permeation. The ability of the formulation to maintain prolonged drug retention on the eye surface is a chief demand for effective accessibility and enhanced permeation through ocular tissues segment [45]. Corneal structure presents a major protective barrier that hinders topical ocular drug permeation. Thus, the enhanced drug corneal permeation can facilitate major pathway for drug entry to anterior chamber, aqueous humor and the deep associated eye tissues. Also, it offers better opportunity for increasing drug access to the posterior eye segment [26].

3.9. *In vivo eye tolerance test (modified Draize test)*

Fig. 8 presents photos of the control rabbit eyes and the test eyes after 2 h of instillation of the last dose of the selected formulations. The investigations of group A, that received FL-CD-Nios/ISG3, showed very slight diffused erythema which resolved after nearly 4 h. However, no other abnormal symptoms were detectable. There was no perceptible corneal swelling, discharge or corneal opacity. Thus, the evaluation score was 1. On the other hand, the score was almost zero for group B that received FL-CD-ERS1/ISG3. The formula did not illicit any inflammation or any other abnormal eye symptoms. The overall *in vivo* evaluation and histopathology studies of the investigated formulations declared that they were well tolerated and suitable for ocular application.

3.10. *Histopatholgical study*

Fig. 9A presents the photomicrography of the untreated cornea. The photomicrograph revealed normal corneal architecture with normal epithelium lining (thick arrow), distinctive nuclei of the corneal cells (thin arrow) and normal collagenous stromal lamellae (star). Fig. 9B and 9C shows the corneal tissue of rabbits that received FL-CD-Nios-Ch/ISG3 and FL-CD-ES1/ISG3, respectively. The photomicrographs revealed normal epithelial lining (thin arrow) and normal corneal stroma. The investigated formulations did not illicit any epithelial or stromal edema. Also, it did not show any inflammation signs. Thus, the investigated formulations were considered to be suitable for ocular application.

3.11. *Corneal visualization using confocal laser scanning microscopy*

CLSM studies were performed in order to appraise the degree of penetration and distribution of the permeated nanocarrier systems through excised cornea. This was accomplished by tracking the fluorescent

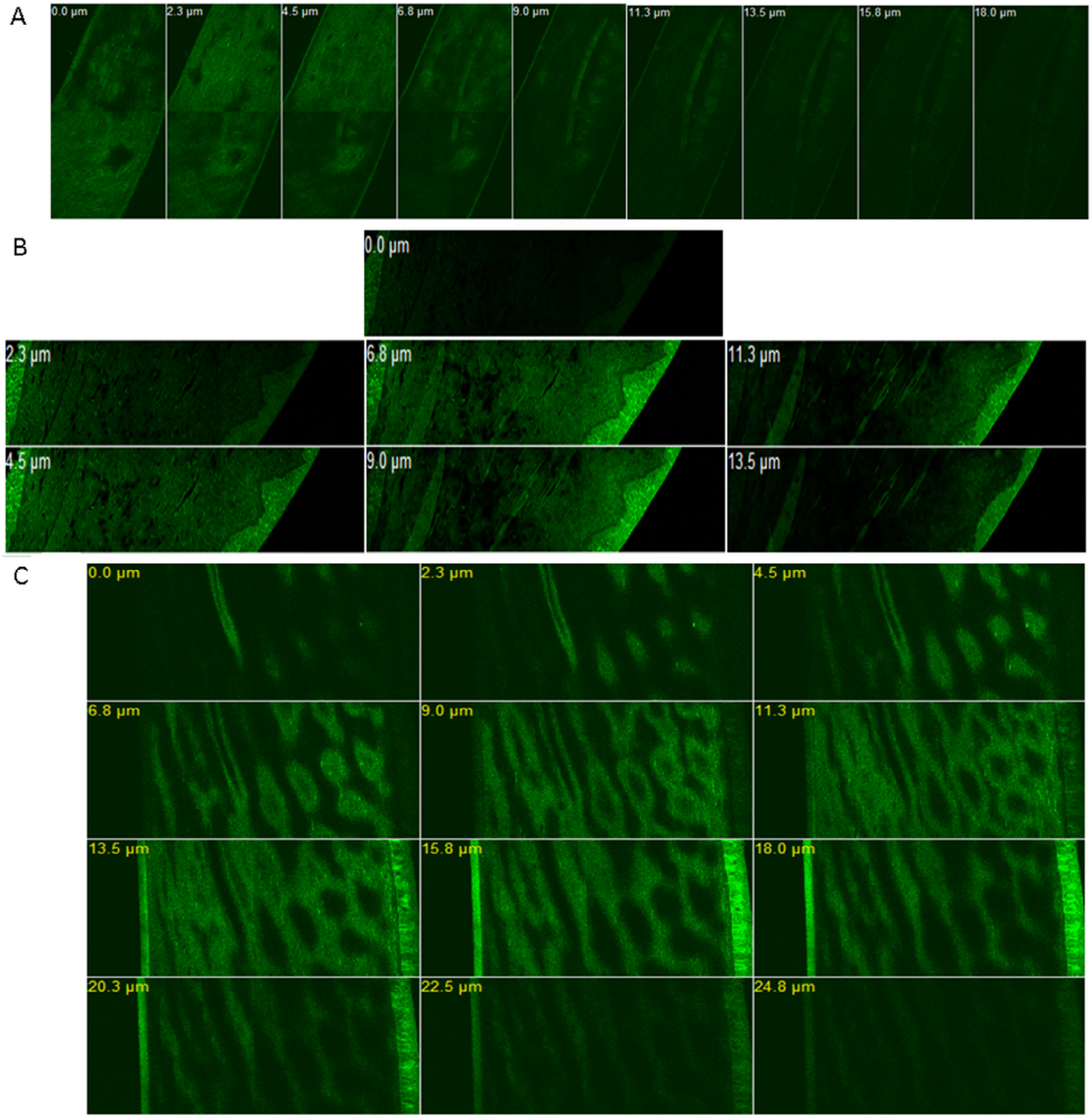

Fig. 10 – CLSM z-stack images of rabbits corneas after 2 h of instilling Rhodamine B fluorescent loaded formulations. Rh B aqueous solution control (A); RhB-Niosomal vesicles/ISG3 (B); Rh B-Eudragit RS1 nanoparticles/ISG3 (C).

marker rhodamine B (RhB) distribution within the corneal tissue layers. The CLSM images Fig. 10 shows the fluorescence images of the corneal layers after 2 h of *in vivo* instilling RhB labeled formulations in the rabbits eyes (group A: RhB-Nios-ch/ISG3; group B: RhB-ERS1/ISG3; group C: RhB aqueous solution). The CLSM images of rabbits corneas for group A and B revealed that the fluorescence was more intense and was distributed throughout the different corneal layers including the superficial epithelial layers, the basal epithelial layers and the collagenous Bowman's layer. Also, the fluorescence distribution was apparent throughout the hydrophilic stroma that consists mainly water. The stroma is the major layer as it constitutes nearly 90% of the corneal layers. Moreover, the intense fluorescence reached the deeper corneal layers – the Descemet's membrane and the endothelium. It can also be depicted that the fluorescence distribution and intensity in group B was more evident than group A. On the other hand, in case of RhB solution fluorescence was less intense with confined distribution to the upper epithelial layers compared to the investigated

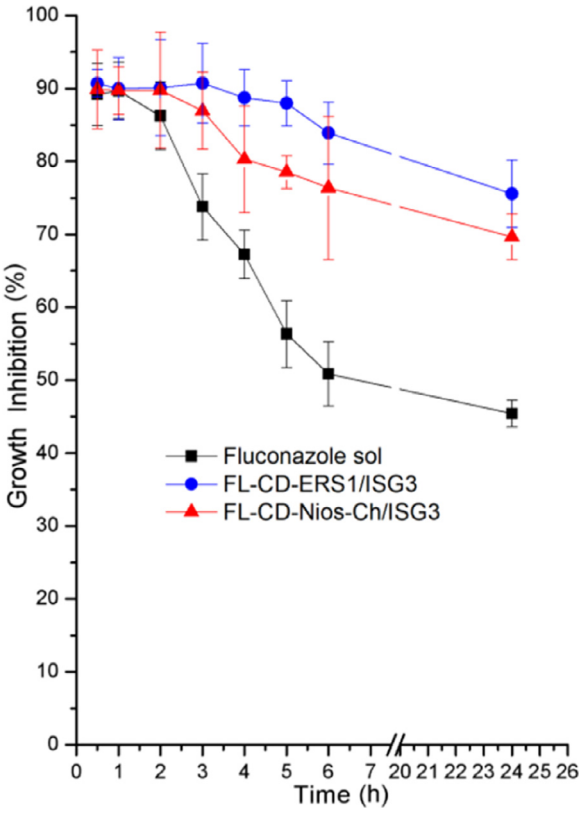

Fig. 11 – Growth inhibition after topical instilling fluconazole aqueous solution, Fl-CD-NIOS/ISG3 and FL-CD-ERS1/ISG3 formulations in rabbits' eyes.

formulations. This indicated the high penetration power of the RhB-loaded Eudragit NPs and niosomal formulations embedded within the *in situ* gel across the different corneal layers – despite that these layers have different hydrophilic and lipophilic nature – in comparison to the aqueous RhB solution.

3.12. *Suceptibility test*

The antifungal activity of FL-CD-Nios-Ch/ISG3 and FL-CD-ES1/ISG3 were investigated in comparison to FL aqueous solution. The percentage inhibition of *Candida albicans* growth was plotted against time. As depicted in Fig. 11 the growth inhibition was maintained at high level in animals groups B and C. These groups received the formulations FL-CD-Nios-Ch/ISG3 and FL-CD-ERS1/ISG3, respectively. On the other hand, the growth inhibition level declined to lower levels in group A that received FL aqueous solution.

The area under the growth inhibition time curve ($AUC_{0-24\,h}$) were calculated. $AUC_{0-24\,h}$ values were 1295.6 ± 39.7, 1818.5 ± 42.4, 1935.7 ± 31.6 for the plain FL aqueous solution, Fl-CD-Nios–Ch/ISG3 and FL-Cd-ERS1/ISG3, respectively. These two formulations exhibited significantly higher ($P < 0.05$) AUC_{0-24h} in comparison to the plain FL aqueous solution. Also, AUC_{0-24h} of FL-CD-ERS1/ISG3 was significantly higher ($P < 0.05$) than that of the FL-CD-Nios-Ch/ISG3. The investigated optimized formulations revealed sustained antifungal activity all over the 24 h study period. It is worthy to note that the antifungal activity relies on several factors including, the drug structure, molecular weight, the available concentration at the intended site of action, the contact duration time with ocular tissues, and the ability to penetrate the cornea [73]. Cyclodextrin complexation has also been reported to decrease drug efflux from cells thus maintain adequate intracellular drug levels to exert the therapeutic effect [74]. Thus, the achieved advance *in vivo* performance of the propsed formulations can be accredited to the combined effects of the positively charged nanocarriers, cyclodextrin complexation and the use of the thermosenstive *in situ* gel.

4. Conclusion

A stepwise optimization strategy was adopted in this study. Our approach included incorporating FL-HP-β-CD complex in the selected optimized Eudragit NPs and chitosan coated niosomal vesicles. The developed formulations were further blended in thermosenstive *in situ* gel. These subsequent steps were conducted to circumvent the limitations of using each of them separately. The developed formulations revealed high entrapment efficiency, nano-sized particles and adequate positive zeta potential. They revealed sustained release, enhanced corneal permeation and satisfactory ocular toleration. They also exhibited sustained high levels of growth inhibition for *Candida albicans*. This new strategy might have contributed in combating the arising incidence of fungal resistance to the drug by offering new nanosized form, of the drug that can escape drug efflux mechanism. Due to the enhanced permeation, the drug could be delivered efficiently to intraocular tissues. This study presents a platform form for further pharmacokinetic studies for evaluating the acheived drug levels in intraocular tissues. Nonetheless, this study offers innovated noninvasive ocular drug delivery systems. The developed formulations can enhance FL ocular absorption, decrease its systemic absorption and minimize its side effects. Moreover, these formulations can be accurately administered in a liquid form which transafer into gel on contacting the eye surface. They could also decrease the drug administration frequency and improve patient compliance. Thus, the adopted approach in this study could possibly lead to better control of serious sight threatening ocular fungal infections.

Conflicts of interest

The authors report no conflict of interests.

Acknowledgment

The authors would like to thank the National Research Centre, Cairo, Egypt for all the facilities and supports.

REFERENCES

[1] Thomas PA, Kaliamurthy J. Mycotic keratitis: epidemiology, diagnosis and management. Clin Microbiol Infect 2013;19(3):210–20.
[2] Joseph J, Sharma S. Antifungal therapy in eye infections: new drugs, new trends. In: Basak A, Chakraborty R, Mandal S, editors. Recent trends in antifungal agents and antifungal therapy. New Delhi: Springer; 2016. p. 217–36.
[3] Li J, Li Z, Liang Z, Han L, Feng H, He S, et al. Fabrication of a drug delivery system that enhances antifungal drug corneal penetration. Drug Deliv 2018;25(1):938–49.
[4] Kathiravan MK, Salake AB, Chothe AS, Dudhe PB, Watode RP, Mukta MS, et al. The biology and chemistry of antifungal agents: a review. Bioorg Med Chem 2012;20(19):5678–98.
[5] Zhang JJ, Xie LK, Chen ZJ, Zhang Q. Pharmacokinetics of topically applied fluconazole in the rabbit eye. Chin J Ophthalmol 2002;38(2):108–11.
[6] Patel A, Cholkar K, Agrahari V, Mitra AK. Ocular drug delivery systems: an overview. World J Pharmacol 2013;2(2):47–64.
[7] Yee RW, Cheng CJ, Meenakshi S, Ludden TM, Wallace JE, Rinaldi MG. Ocular penetration and pharmacokinetics of topical fluconazole. Cornea 1997;16(1):64–71.
[8] Abdel-Rhaman MS, Soliman W, Habib F, Fathalla D. A new long-acting liposomal topical antifungal formula: human clinical study. Cornea 2012;31(2):126–9.
[9] Habib FS, Fouad EA, Abdel-Rhaman MS, Fathalla D. Liposomes as an ocular delivery system of fluconazole: *in vitro* studies. Acta Ophthalmol 2010;88(8):901–4.
[10] El-Nesr OH, Yahiya SA, El-Gazayerly ON. Effect of formulation design and freeze-drying on properties of fluconazole multilamellar liposomes. SPJ 2010;18(4):217–24.
[11] Liu J, Fu S, Wei N, Hou Y, Zhang X, Cui H. The effects of combined menthol and borneol on fluconazole permeation through the cornea *ex vivo*. Eur J Pharmacol 2012;688(1–3):1–5.
[12] Kaur IP, Rana C, Singh M, Bhushan S, Singh H, Kakkar S. Development and evaluation of novel surfactant-based elastic vesicular system for ocular delivery of fluconazole. J Ocul Pharmacol Ther 2012;28(5):484–96.
[13] Coneac G, Vlaia V, Olariu I, Muţ AM, Anghel DF, Ilie C, et al. Development and evaluation of new microemulsion-based hydrogel formulations for topical delivery of fluconazole. AAPS PharmSciTech 2015;16(4):889–904.
[14] Gratieri T, Gelfuso GM, de Freitas O, Rocha EM, Lopez RFV. Enhancing and sustaining the topical ocular delivery of fluconazole using chitosan solution and poloxamer/chitosan in situ forming gel. Eur J Pharm Biopharm 2011;79(2):320–7.
[15] Lihong W, Xin C, Yongxue G, Yiying B, Gang C. Thermoresponsive ophthalmic poloxamer/tween/carbopol in situ gels of a poorly water-soluble drug fluconazole: preparation and *in vitro-in vivo* evaluation. Drug Dev Ind Pharm 2014;40(10):1402–10.
[16] Pathak MK, Chhabra G, Pathak K. Design and development of a novel pH triggered nanoemulsified in-situ ophthalmic gel of fluconazole: *ex vivo* transcorneal permeation, corneal toxicity and irritation testing. Drug Dev Ind Pharm 2013;39(5):780–90.
[17] Mohammed N, Rejinold NS, Mangalathillam S, Biswas R, Nair SV, Jayakumar R. Fluconazole loaded chitin nanogels as a topical ocular drug delivery agent for corneal fungal infections. J Biomed Nanotechnol 2013;9(9):1521–31.
[18] Fernández-Ferreiro A, Fernández Bargiela N, Varela MS, Martínez MG, Pardo M, Piñeiro Ces A, et al. Cyclodextrin-polysaccharide-based, in situ-gelled system for ocular antifungal delivery. Beilstein J Org Chem 2014;10:2903–11.
[19] Fetih G. Fluconazole-loaded niosomal gels as a topical ocular drug delivery system for corneal fungal infections. J Drug Deliv Sci Technol 2016;35:8–15.
[20] Alpana R, Pooja MR, Nitish K, Rakesh R. Comparative study of eudragit RS100 and RL100 nanoparticles as ophthalmic vehicle for fungal infection. Pharm Nanotechnol 2016;4(4):316–28.
[21] Moustafa MA, Elnaggar YSR, El-Refaie WM, Abdallah OY. Hyalugel-integrated liposomes as a novel ocular nanosized delivery system of fluconazole with promising prolonged effect. Int J Pharm 2017;534(1):14–24.
[22] Moustafa MA, El-Refaie WM, Elnaggar YSR, Abdallah OY. Gel in core carbosomes as novel ophthalmic vehicles with enhanced corneal permeation and residence. Int J Pharm 2018;546(1):166–75.
[23] Kelidari HR, Moazeni M, Babaei R, Saeedi M, Akbari J, Parkoohi PI, et al. Improved yeast delivery of fluconazole with a nanostructured lipid carrier system. Biomed Pharmacother 2017;89:83–8.
[24] Durand ML. Bacterial and fungal endophthalmitis. Clin Microbiol Rev 2017;30(3):597–613.
[25] Moazeni M, Kelidari HR, Saeedi M, Morteza-Semnani K, Nabili M, Gohar AA, et al. Time to overcome fluconazole resistant candida isolates: solid lipid nanoparticles as a novel antifungal drug delivery system. Colloids Surf B Biointerfaces 2016;142:400–7.
[26] Loftsson T, Stefánsson E. Cyclodextrins and topical drug delivery to the anterior and posterior segments of the eye. Int J Pharm 2017;531(2):413–23.
[27] Weng Y, Liu J, Jin S, Guo W, Liang X, Hu Z. Nanotechnology-based strategies for treatment of ocular disease. Acta Pharm Sin B 2017;7(3):281–91.
[28] Challa R, Ahuja A, Ali J, Khar RK. Cyclodextrins in drug delivery: an updated review. AAPS PharmSciTech 2005;6(2):E329–57.
[29] Loftsson T, Stefansson E. Cyclodextrins in eye drop formulations: enhanced topical delivery of corticosteroids to the eye. Acta Ophthalmol Scand 2002;80(2):144–50.
[30] Loftsson T, Stefánsson E. Cyclodextrins in ocular drug delivery: theoretical basis with dexamethasone as a sample drug. J Drug Deliv Sci Technol 2007;17(1):3–9.
[31] Loftssona T, Jarvinen T. Cyclodextrins in ophthalmic drug delivery. Adv Drug Deliv Rev 1999;36(1):59–79.
[32] Rajewski RA, Stella VJ. Pharmaceutical applications of cyclodextrins. 2. *in vivo* drug delivery. J Pharm Sci 1996;85(11):1142–69.
[33] Tiwari G, Tiwari R, Rai AK. Cyclodextrins in delivery systems: applications. J Pharm Bioall Sci 2010;2(2):72–9.
[34] Gharib R, Greige-Gerges H, Fourmentin S, Charcosset C, Auezova L. Liposomes incorporating cyclodextrin-drug inclusion complexes: current state of knowledge. Carbohydr Polym 2015;129:175–86.
[35] Gidwani B, Vyas A. A comprehensive review on cyclodextrin-based carriers for delivery of chemotherapeutic cytotoxic anticancer drugs. Biomed Res Int 2015;2015:198268.
[36] Mennini N, Cirri M, Maestrelli F, Mura P. Comparison of liposomal and nlc (nanostructured lipid carrier) formulations for improving the transdermal delivery of oxaprozin: effect of cyclodextrin complexation. Int J Pharm 2016;515(1):684–91.
[37] Shelley H, Babu RJ. Role of cyclodextrins in nanoparticle-based drug delivery systems. J Pharm Sci 2018;107(7):1741–53.
[38] Tang P, Sun Q, Zhao L, Pu H, Yang H, Zhang S, et al. Mesalazine/hydroxypropyl-beta-cyclodextrin/chitosan nanoparticles with sustained release and enhanced anti-inflammation activity. Carbohydr Polym 2018;198:418–25.
[39] Ruckmani K, Sankar V. Formulation and optimization of

zidovudine niosomes. AAPS PharmSciTech 2010;11(3):1119–27.
[40] Katara R, Majumdar DK. Eudragit RL100-based nanoparticulate system of aceclofenac for ocular delivery. Colloid Surf B Biointerfaces 2013;103:455–62.
[41] Li J, Zhang S, Zhou Y, Guan S, Zhang L. Inclusion complexes of fluconazole with β-cyclodextrin and 2-hydroxypropyl-β-cyclodextrin in aqueous solution: preparation, characterization and a structural insight. J Incl Phenom Macrocycl Chem 2016;84(3):209–17.
[42] Yurtdaş G, Demirel M, Genç L. Inclusion complexes of fluconazole with β-cyclodextrin: physicochemical characterization and in vitro evaluation of its formulation. J Incl Phenom Macrocycl Chem 2011;70(3):429–35.
[43] Ammar HO, Salama HA, El-Nahhas SA, Elmotasem H. Design and evaluation of chitosan films for transdermal delivery of glimepiride. Curr Drug Deliv 2008;5(4):290–8.
[44] Zubairu Y, Negi LM, Iqbal Z, Talegaonkar S. Design and development of novel bioadhesive niosomal formulation for the transcorneal delivery of anti-infective agent: *in vitro* and *ex vivo* investigations. Asian J Pharm Sci 2015;10(4):322–30.
[45] Hao J, Wang X, Bi Y, Teng Y, Wang J, Li F, et al. Fabrication of a composite system combining solid lipid nanoparticles and thermosensitive hydrogel for challenging ophthalmic drug delivery. Colloids Surf B Biointerfaces 2014;114:111–20.
[46] Morsi N, Ghorab D, Refai H, Teba H. Ketoroloac tromethamine loaded nanodispersion incorporated into thermosensitive in situ gel for prolonged ocular delivery. Int J Pharm 2016;506(1–2):57–67.
[47] Mahmoud AA, El-Feky GS, Kamel R, Awad GE. Chitosan/sulfobutylether-beta-cyclodextrin nanoparticles as a potential approach for ocular drug delivery. Int J Pharm 2011;413(1–2):229–36.
[48] Khan KA. The concept of dissolution efficiency. J Pharm Pharmacol 1975;2:48–9.
[49] Dash S, Murthy PN, Nath L, Chowdhury P. Kinetic modeling on drug release from controlled drug delivery systems. Acta Pol Pharm 2010;67(3):217–23.
[50] Peppas NA, Sahlin JJ. A simple equation for the description of solute release. III. coupling of diffusion and relaxation. Int J Pharm 1989;57(2):169–72.
[51] Costa P, Sousa Lobo JM. Modeling and comparison of dissolution profiles. Eur J Pharm Sci 2001;13(2):123–33.
[52] Hiremath PS, Saha RN. Controlled release hydrophilic matrix tablet formulations of isoniazid: design and in vitro studies. AAPS PharmSciTech 2008;9(4):1171–8.
[53] Kassem AA, Abd El-Alim SH, Asfour MH. Enhancement of 8-methoxypsoralen topical delivery via nanosized niosomal vesicles: formulation development, *in vitro* and *in vivo* evaluation of skin deposition. Int J Pharm 2017;517(1–2):256–68.
[54] ElMeshad AN, Mohsen AM. Enhanced corneal permeation and antimycotic activity of itraconazole against candida albicans via a novel nanosystem vesicle. Drug Deliv 2016;23(7):2115–23.
[55] Salama AH, Shamma RN. Tri/tetra-block co-polymeric nanocarriers as a potential ocular delivery system of lornoxicam: *in vitro* characterization, and in vivo estimation of corneal permeation. Int J Pharm 2015;492(1–2):28–39.
[56] Sharma UK, Verma A, Prajapati SK, Pandey H, Pandey AC. *In vitro*, *in vivo* and pharmacokinetic assessment of amikacin sulphate laden polymeric nanoparticles meant for controlled ocular drug delivery. Appl Nanosci 2015;5(2):143–55.
[57] Das S, Suresh PK, Desmukh R. Design of eudragit RL100 nanoparticles by nanoprecipitation method for ocular drug delivery. Nanomedicine 2010;6(2):318–23.
[58] Dash AK, Elmquist WF. Fluconazole. In: Brittain HG, editor. Analytical profiles of drug substances and excipients. Academic Press; 2001. p. 67–113.
[59] Budhian A, Siegel SJ, Winey KI. Haloperidol-loaded plga nanoparticles: systematic study of particle size and drug content. Int J Pharm 2007;336(2):367–75.
[60] Maestrelli F, González-Rodríguez ML, Rabasco AM, Ghelardini C, Mura P. New "drug-in cyclodextrin-in deformable liposomes" formulations to improve the therapeutic efficacy of local anaesthetics. Int J Pharm 2010;395(1):222–31.
[61] Fatouros DG, Hatzidimitriou K, Antimisiaris SG. Liposomes encapsulating prednisolone and prednisolone-cyclodextrin complexes: comparison of membrane integrity and drug release. Eur J Pharm Sci 2001;13(3):287–96.
[62] Gratieri T, Gelfuso GM, Rocha EM, Sarmento VH, de Freitas O, Lopez RFV. A poloxamer/chitosan in situ forming gel with prolonged retention time for ocular delivery. Eur J Pharm Biopharm 2010;75(2):186–93.
[63] El-Kamel AH. *In vitro* and *in vivo* evaluation of pluronic F127-based ocular delivery system for timolol maleate. Int J Pharm 2002;241(1):47–55.
[64] Chen H, Gao J, Wang F, Liang W. Preparation, characterization and pharmacokinetics of liposomes-encapsulated cyclodextrins inclusion complexes for hydrophobic drugs. Drug Deliv 2007;14(4):201–8.
[65] Zhang K, Shi X, Lin X, Yao C, Shen L, Feng Y. Poloxamer-based in situ hydrogels for controlled delivery of hydrophilic macromolecules after intramuscular injection in rats. Drug Deliv 2015;22(3):375–82.
[66] Jain SK, Gupta Y, Jain A, Bhola M. Multivesicular liposomes bearing celecoxib-β-cyclodextrin complex for transdermal delivery. Drug Deliv 2007;14(6):327–35.
[67] McCormack B, Gregoriadis G. Drugs-in-cyclodextrins-in-liposomes: an approach to controlling the fate of water insoluble drugs in vivo. Int J Pharm 1998;162(1):59–69.
[68] Loftsson T. Self-assembled cyclodextrin nanoparticles and drug delivery. J Incl Phenom Macrocycl Chem 2014;80(1):1–7.
[69] Gavini E, Spada G, Rassu G, Cerri G, Brundu A, Cossu M, et al. Development of solid nanoparticles based on hydroxypropyl-beta-cyclodextrin aimed for the colonic transmucosal delivery of diclofenac sodium. J Pharm Pharmacol 2011;63(4):472–82.
[70] Oommen E, Tiwari SB, Udupa N, Kamath R, Devi PU. Niosome entrapped β-cyclodextrin methotrexate complex as a drug delivery system. Indian J Pharmacol 1999;31(4):279–84.
[71] Spada G, Gavini E, Cossu M, Rassu G, Giunchedi P. Solid lipid nanoparticles with and without hydroxypropyl-beta-cyclodextrin: a comparative study of nanoparticles designed for colonic drug delivery. Nanotechnology 2012;23(9):095101.
[72] Jansook P, Ogawa N, Loftsson T. Cyclodextrins: structure, physicochemical properties and pharmaceutical applications. Int J Pharm 2018;535(1–2):272–84.
[73] Manzouri B, Vafidis GC, Wyse RK. Pharmacotherapy of fungal eye infections. Expert Opin Pharmacother 2001;2(11):1849–57.
[74] Zhang Y, Meng FC, Cui YL, Song YF. Enhancing effect of hydroxypropyl-beta-cyclodextrin on the intestinal absorption process of genipin. J Agric Food Chem 2011;59(20):10919–26.